

FNS: an event-driven spiking neural network framework for efficient simulations of large-scale brain models[☆]

preprint version

Gianluca Susi^{a,b,*}, Pilar Garcés^a, Alessandro Cristini^c, Emanuele Paracone^b,
Mario Salerno^c, Fernando Maestú^{a,d}, Ernesto Pereda^{a,e}

^a*Laboratory of Cognitive and Computational Neuroscience, Center for Biomedical Technology, Complutense University of Madrid & Technical University of Madrid, Spain*

^b*Department of Civil Engineering and Computer Science, University of Rome “Tor Vergata”, Italy*

^c*Department of Electronic Engineering, University of Rome “Tor Vergata”, Italy*

^d*Department of Basic Psychology II, Faculty of Psychology, Complutense University of Madrid, Spain*

^e*Department of Industrial Engineering, IUNE, University of La Laguna, Spain*

Abstract

Limitations in processing capabilities and memory of today’s computers make spiking neuron-based (human) whole-brain simulations inevitably characterized by a compromise between bio-plausibility and computational cost. It translates into brain models composed of a reduced number of neurons and a simplified neuron’s mathematical model.

Taking advantage of the sparse character of brain-like computation, *event-driven* technique allows us to carry out efficient simulation of large-scale *Spiking Neural Networks* (SNN). The recent *Leaky Integrate-and-Fire with Latency* (LIFL) spiking neuron model is event-driven compatible and exhibits some realistic neuronal features, opening new horizons in whole-brain modelling. In this paper we present FNS, a LIFL-based *exact* event-driven spiking neural network framework implemented in *Java* and oriented to whole-

[☆]*FNS* software and documentation are available freely at www.fnsneuralsimulator.org

*Corresponding author: Gianluca Susi. Laboratory of Cognitive and Computational Neuroscience, Center for Biomedical Technology, Complutense University of Madrid & Technical University of Madrid; Department of Civil Engineering and Computer Science, University of Rome ‘Tor Vergata’

Email address: gianluca.susi@ctb.upm.es (Gianluca Susi)

brain simulations. FNS combines spiking/synaptic whole-brain modelling with the event-driven approach, allowing us to define heterogeneous modules and multi-scale connectivity with delayed connections and plastic synapses, providing fast simulations at the same time. A novel parallelization strategy is also implemented in order to further speed up simulations.

This paper presents mathematical models, software implementation and simulation routines on which FNS is based. Finally, a reduced brain network model (1400 neurons and 45000 synapses) is synthesized on the basis of real brain structural data, and the resulting model activity is compared with associated brain functional (source-space MEG) data. The conducted test shows a good matching between the activity of model and that of the emulated subject, in outstanding simulation times (about 20s for simulating 4s of activity with a normal PC).

Dedicated sections of stimuli editing and output synthesis allow the neuroscientist to introduce and extract brain-like signals, respectively. The possibility to activate *spike-timing-dependent plasticity* (STDP) permits to study the longitudinal implications of specific structure modifications on global brain activity, and vice versa.

The parallel software architecture allows us to deal with the plethora of possible applications using multi-thread implementations.

Keywords: Event-driven Simulation, Leaky Integrate-and-Fire with Latency (LIFL), Large-scale Spiking Neural Network, Functional connectivity, Diversity, Magnetoencephalography

1. Introduction

Today's advanced *magnetic resonance imaging* (MRI) -based techniques allow a thorough estimation of the structural *connectome* (i.e., the map of neural connections in the brain) (Hagmann, 2005; Sporns et al., 2005). Motivated by this recent opportunity, more and more researchers carry out the synthesis of brain dynamic models using approaches based on graph theory, achieving the reproduction of brain oscillations (e.g. Cabral et al., 2011; Nakagawa et al., 2014; Cabral et al., 2014), as well as the emulation of task execution (e.g. Scheffler, 2015; Gollo et al., 2016). In such approaches, *nodes* represent surrogates of brain regions (corresponding to *gray matter*), and *edges* represent the long-range connections, along fibre tracts, between them (corresponding to *white matter*), usually estimated using *diffusion tensor*

imaging (DTI) (Fig. 1).

Current literature on the synthesis of brain activity using real structural brain data shows the feasibility of reproducing brain activity revealed by functional imaging techniques such as *Multi-Unit Activity* (MUA) and *Local Field Potential* (LFP) (Barardi et al., 2014), *functional MRI* (Deco and Jirsa, 2012) and *Magnetoencephalography* (MEG) (Nakagawa et al., 2014; Cabral et al., 2014), demonstrating the capability of resulting dynamic models to provide insight into brain operation, thus suitable for discovering the mechanistic underpinnings of the relationship between structural connectivity (SC, i.e. the network of anatomical connections between distinct brain regions) and functional connectivity (FC, i.e. the network of functional interactions between distinct brain regions).

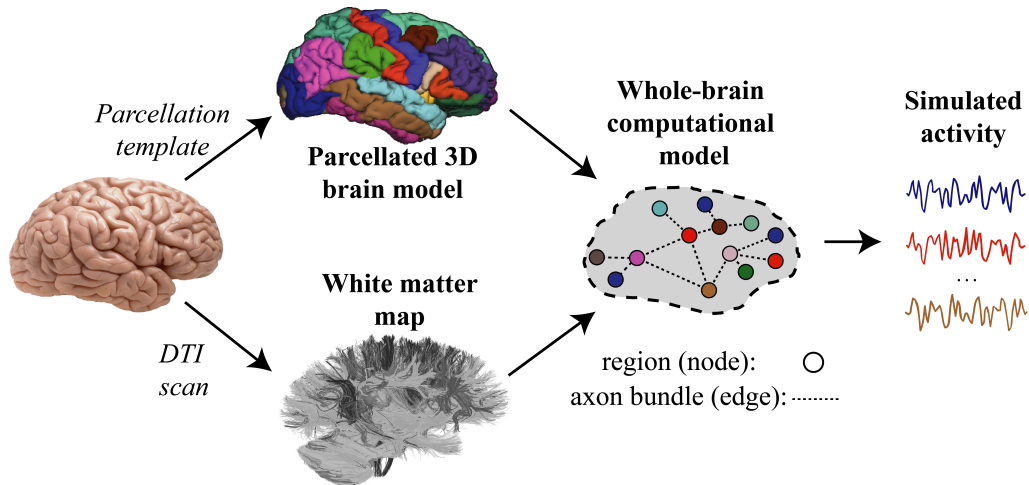


Figure 1. Synthesis of a computational brain model using the graph approach. White matter connections can be extracted by means of DTI. Brains of individual subjects can be coregistered to a parcellation template (*atlas*) in order to assign connections to specific brain areas. By assigning node local dynamics to the obtained *structural connectome*, it is possible to extract simulated activity. The number of nodes of the model depends on the template used, and each node can be represented at different levels of abstraction (e.g., ensemble of spiking neurons).

Nodes can be represented at different levels of abstraction (Deco et al., 2008; Cabral et al., 2014; Gollo et al., 2014): *neural mass* and *neural field* models (David and Friston, 2003; Coombes, 2006; Pinotsis et al., 2014) sacrifice realism for a more parsimonious description of key mechanisms (David and Friston, 2003), whereas *spiking/synaptic models* (Vicente et al., 2008;

Nakagawa et al., 2014; Maslennikov and Nekorkin, 2014; Gollo et al., 2010) present a higher degree of freedom, which gives rise to highly complex and realistic behaviours on a broad frequency range of the related oscillations (Barardi et al., 2014). In addition, spiking/synaptic models offer the opportunity to relate to real-brain data transversely (*micro-*, *meso-*, and *macro-scale*, referring to the categorisation of Bohland et al., 2009), as well as to implement STDP, resulting indispensable in many kinds of computational neuroscience studies (Pecevski et al., 2014).

On the other hand, spiking/synaptic-based whole-brain simulations are extremely expensive from a computational point of view (Izhikevich, 2004). This issue translates to the use of simplified spiking neuron models, and (often identical) nodes composed of a low number of elements, thereby reducing the realism of the overall brain model.

Neuron models are described by differential equations and usually simulated with clock-driven (synchronous) algorithms, by means of proper integration methods (see Brette et al., 2007, for an extensive review). In this way the update is done at every tick of a clock $\mathbf{X}(t) \rightarrow \mathbf{X}(t + dt)$, and involves all network elements (neurons and possibly synapses). In general, such two peculiarities make the simulation not *exact* (entailing missing spikes), and cause a fast growth of simulation times/occupied memory when the network size increases.

Conversely, in the event-driven (or asynchronous) approach a network element is updated only when it receives or emits a spike. Then, such approach does not envisage a periodic update, neither a check of all network elements, producing simulations devoid of missed spikes, and exploits the sparseness of brain-like activity. Since the latter is irregular in time with low average (Mouraud and Puzenat, 2009), this approach leads to a considerable reduction of computational costs for large-scale network simulations (Ros et al., 2006). Nevertheless, the need of an explicit solution for the neuron state between spikes, and the consideration of incoming and outgoing pulses as discrete events, make the event-driven simulation of classic bio-realistic models very challenging. This has stimulated a big interest in scientific community to develop both realistic and event-driven-compatible spiking neuron models (see Brette, 2006, 2007; Tonnelier et al., 2007; Salerno et al., 2011; Rudolph-Lilith et al., 2012), SNN event-driven simulators (see Pecevski et al., 2014; Cristini et al., 2015), as well as hybrid *event/time-step* based simulation strategies (see Morrison et al., 2006; Hanuschkin et al., 2010; D’Haene et al., 2014; Gewaltig and Diesmann, 2007; Brette and Goodman, 2016). The

event-driven technique is steadily overcoming the classic bioplausibility/complexity trade-off of time-driven simulations.

In particular, the *Leaky Integrate-and-Fire with Latency* (LIFL) model is a recent neuron model that can be simulated in event-driven fashion, preserving important computational features at the same time (Salerno et al., 2011; Cardarilli et al., 2013; Cristini et al., 2015; Susi, 2015; Susi et al., 2016; Acciarito et al., 2017). Differently from the *Leaky Integrate-and-Fire* (LIF), LIFL incorporates important neuronal features extracted from the bio-realistic *Hodgkin-Huxley* (HH) model, such as the *spike latency* (FitzHugh, 1955; Izhikevich, 2004), that has been proved to be fundamental in many scenarios of neural computation, providing a large range of behaviors. Then LIFL may represent an optimal choice for the efficient simulation of large scale brain models.

In this work we present FNS (literally, *Firnet NeuroScience*), a LIFL-based exact event-driven SNN framework oriented to whole-brain simulations, implemented in *Java*. FNS allows us to generate brain network models on the basis of a versatile graph-based multi-scale neuroanatomical connectivity scheme, allowing for heterogeneous neuron modules and connections. In addition to the high-customizability of the network, proper input and output sections make it possible to relate model activity to real functional data, and plasticity can make the network parameters evolve depending on the network activity. The efficient computation and a novel parallelization method provide fast simulations even for whole-brain models, without the need of a supercomputer.

In section 2, we describe the neurobiological principles and mathematical models on which FNS is based: neuron model, region model, fibre tracts model, plasticity, input and output signals, contextualized to the proposed event-driven technique.

In section 3, we present the environment that the framework offers for the synthesis of custom models and the design of specific simulations: generator section, neuroanatomical model section and output section.

In section 4, we illustrate the technical aspects of the simulation framework itself: design principles, data structures and parallelization strategy.

In section 5, we present a simulation example to show how to conduct a simulation in FNS, and evaluate the realism and performances of the framework itself. In short, we will synthesize a brain model on the basis of structural data; from this we synthesize electrophysiological-like output signals and compare with associated functional real data.

In the Conclusion section, we summarize the main conclusion of the study and envisage the wide range of possible applications of FNS.

In this manuscript, a single neuron is indicated with n ; an axonal connection between two whichever neurons with e ; a neuron module (corresponding to a region or subregion in real case) with N , and called *network node*; the complete set of connections between two nodes (corresponding to fibre tracts in real case) with E , and called *network edge*.

The main scope of this paper is to present the operation aspects of FNS to the reader. The software can be freely downloaded at www.fnsneuralsimulator.org in order to create new models and conduct new experiments. A user guide in PDF is also provided with the software in the download link.

2. From neurobiology to mathematical models

Specificity and heterogeneity characterize the human brain at all scales. In this regard, recent works highlight crucial aspects that have to be taken into account in brain models to obtain realistic dynamics:

- *Region bioplausibility*: in spiking/synaptic models, an inappropriate choice of the spiking neuron model or the intra-node connectivity may lead to results having nothing to do with the information processing of real brain (Izhikevich, 2004). Of course, also node cardinality is important for achieving an appropriate global behaviour.
- *Region diversity*: diversity among and within regions specializes the behaviour of single parts of the network, enhancing the information content and coding performances and shaping properties of collective behavior such as synchronization (see Thivierge, 2008; Gollo et al., 2016).
- *Inter-region connection bioplausibility*: synchronization between network nodes is strongly sensitive to edge parameters (as weights, delays and connection number) and their distributions (Vicente et al., 2008; Viriyopase et al., 2012; Gollo et al., 2014).
- *Inter-region connection diversity*: selective variations of such parameters are able to reconfigure the network synchronization profile (Abuhassan et al., 2014), including synchronization between nodes that are not directly connected to the modified edge Gollo et al. (2014).

A simulation framework should guarantee the possibility to take into account such aspects in order to avoid the alteration of the network operation. In this section we present mathematical models used by FNS to implement such possibilities.

2.1. LIFL Neuron model

Large-scale network simulations are frequently carried out with the classic LIF model because it is very fast to simulate. On the other hand, such model has been regarded as unrealistically simple, thereby incapable of reproducing the dynamics exhibited by cortical neurons (Izhikevich, 2003). If the goal is to synthesize a computational model of the brain, a greater level of biological plausibility is required (Izhikevich, 2004).

FNS is based on the LIFL, that besides being computationally simple it is also able to support a greater number of neuronal features than the LIF.

2.1.1. A brief introduction to the spike latency neuro-computational feature

Among all the neuron features, the *spike latency* (i.e., the membrane potential-dependent delay time between the overcoming of the “threshold” potential and the actual spike generation (Izhikevich, 2004)) is of considerable importance because it extends the neuron computation capabilities over the “threshold”, giving rise to a range of new behaviors. Spike latency is ubiquitous in the nervous system, including the auditory, visual, and somatosensory systems (Wang et al., 2013; Trotta et al., 2013).

From a computational point of view it provides a spike-timing mechanism to encode the strength of the input (Izhikevich, 2007) conferring many coding/decoding capabilities to the network (e.g., Gollisch and Meister, 2008; Fontaine and Peremans, 2009; Susi, 2015), whereas, from a statistical point of view it results in a desynchronizing effect (Salerno et al., 2011; Cardarilli et al., 2013), fostering the emergence of higher frequencies (Susi et al., 2016) and providing robustness to noise (Izhikevich, 2007, chapter 7) to the network. Spike latency has already been introduced in some variants of the LIF, as *QIF* (Vilela and Lindner, 2009) and *EIF* (Fourcaud-Trocme et al., 2003). In LIFL spike latency is embedded with a mechanism extracted from the realistic HH model (Salerno et al., 2011), both simple and suitable to the event-driven simulation strategy

2.1.2. LIFL operation

In this section, we briefly describe the behaviour of the LIFL neuron model. For the sake of simplicity, we will refer to its basic configuration;

however, we also present some strategies to increase the realism and implement further neuronal features.

LIFL neuron model is characterized by a real non-negative quantity S (the *inner state*, corresponding to the membrane potential of the biological neuron), which is defined from 0 (corresponding to the resting potential of the biological neuron) to S_{max} (*maximum state*), a value much greater than one, at most ∞ . Simple Dirac delta functions (representing the action potentials) are supposed to be exchanged between network's neurons, in form of *pulses* or pulse trains. The model is able to operate in two different modes: *passive mode* when $S < S_{th}$, and *active mode* when $S \geq S_{th}$, where S_{th} is the *firing threshold*, a value slightly greater than 1. In passive mode, S is affected by a decay, whereas active mode is characterized by a spontaneous growth of S . Assuming that neuron n_j (i.e., the *burning neuron*) is receiving a pulse from neuron n_i (i.e., the *firing neuron*), its inner state is updated through one of the following equations, depending on whether n_j was in passive or in active mode, respectively:

$$S_j = \begin{cases} S_{p_j} + A_i \cdot W_{i,j} - T_l, & \text{for } 0 \leq S_{p_j} < S_{th} & (1a) \\ S_{p_j} + A_i \cdot W_{i,j} + T_r, & \text{for } S_{th} \leq S_{p_j} < S_{max} & (1b) \end{cases}$$

S_{p_j} represents the burning neuron's *previous state*, i.e., the inner state immediately before the new pulse arrives. A_i represents the *presynaptic amplitude*, which is related to the firing neuron, and it can take two values: A_{exc} (a positive value) or A_{inh} (a negative value) depending on whether the neuron is excitatory or inhibitory, respectively; note that A_{exc} and A_{inh} are global parameters of the model. $W_{i,j}$ represents the *synaptic weight* related to the connection from neuron i to neuron j (in this paper, w or ω will be used instead of W , depending on the connection is inter- or intra- node, respectively); if this quantity is equal to 0, the related connection is not present. The product $A_i \cdot W$ globally represents the amplitude of the pulse arriving to the burning neuron n_j (i.e., the *synaptic pulse*) from the firing neuron n_i . Note that the same neuron can be considered firing or burning, depending on whether it is emitting or receiving a pulse.

T_l (the *leakage term*) takes into account the behaviour of S during two consecutive input pulses in passive mode. Specifically, for a LIFL basic configuration the simple case of linear subthreshold decay can be chosen (as in Mattia and Del Giudice, 2000), assuming $T_l = D\Delta t$, in which D is the *decay parameter*, and Δt represents the temporal distance between a couple of

consecutive incoming spikes. Of course, D should be greater than 0 (if it is 0, no decay is applied in passive mode, and the neuron behaves as a *perfect integrator*).

T_r (the *rise term*) takes into account the overthreshold growth acting upon S during two consecutive input pulses in active mode. Specifically, once the neuron’s inner state crosses the threshold, the neuron is ready to fire. The firing is not instantaneous, but it occurs after a continuous-time delay, representing the spike latency, that we call *time-to-fire* and indicate with t_f in our model. This quantity can be affected by further inputs, making the neuron sensitive to changes in the network spiking activity for a certain time window, until the actual spike generation. S and t_f are related through the following bijective relationship, called the *firing equation*:

$$t_f = \frac{a}{(S - 1)} - b \quad (2)$$

where $a, b \geq 0$. Such rectangular hyperbola has been obtained through the simulation of a membrane patch stimulated by brief current pulses (i.e., 0.01 *ms* of duration), solving the Hodgkin-Huxley equations (Hodgkin and Huxley, 1952) in *NEURON* environment (Hines and Carnevale, 1997), as described in Salerno et al. (2011). Conversely to previous definitions of LIFL (Salerno et al., 2011; Cristini et al., 2015), positive constants a and b have been introduced in order to make the model able to encompass a greater number of neuron types; in particular, a allows us to distance/approach the hyperbola to its centre, while b allows us to define a S_{max} , conferring a biophysical meaning to the inner state in active mode (note that if $b = 0$, then $S_{max} = \infty$; nevertheless, the in/out behaviour remains realistic).

The firing equation is a simple bijective relationship between S and t_f , and this mathematical structure allows us to match the latency curves of different neurons, without adding computational cost. Then, if the inner state of a neuron is known, the related t_f can be exactly calculated by means of Eq. 2. As introduced in 2.1.1, this nonlinear trend has been observed in most cortical neurons (Izhikevich, 2004); similar behaviors have been found by other authors, such as Wang et al. (2013) and Trotta et al. (2013), using DC inputs.

The firing threshold can be equivalently written as:

$$S_{th} = 1 + c \quad (3)$$

where c is a positive value called *threshold constant*, that fixes a bound

for the maximum t_f . According to Eq. 3, when $S = S_{th}$, the t_f is maximum, and equal to:

$$t_{f,max} = a/c - b \quad (4)$$

where $t_{f,max}$ represents the upper bound of the time-to-fire. As mentioned above, the latter consideration is crucial in order to have a finite maximum spike latency as in biological neurons (FitzHugh, 1955). From the last equation, we obtain the restriction $c < a/b$.

Using Eq. 2 under proper considerations (see *Appendix A*), it is possible to obtain T_r (*rise term*), as follows:

$$T_r = \frac{(S_p - 1)^2 \Delta t}{a - (S_p - 1) \Delta t} \quad (5)$$

in which S_p represents the previous state, whereas Δt is the temporal distance between two consecutive incoming presynaptic spikes. The Eq. 5 allows us to determine the inner state of a burning neuron at the time that it receives further inputs during the t_f time window. In Fig. 2, the operation of LIFL is illustrated, while the effect of Eq. 5 is shown in Fig. 3.

Assuming that an input spike leads the inner state underthreshold at time t_A , the arrival of a contribution during the latency time (i.e., at time t_B) results in a new t_f (i.e., a change of the firing time). Excitatory (inhibitory) inputs increase (decrease) the inner state of a burning neuron. Therefore, when a neuron is in active mode, excitatory (inhibitory) inputs decrease (increase) the related time-to-fire (*post-trigger anticipation/postponement* respectively). If the inhibitory effect is as strong as to pull the burning neuron state under the firing threshold, its t_f will be suppressed and its state will come back to the passive mode (*post-trigger inhibition*) (Salerno et al., 2011; Cristini et al., 2015).

For a given neuron j in active mode, the arrival of new input contributions provokes t_f updating. Once the t_f is reached, the output spike is generated and the inner state is reset. Note that if incoming spikes are such as to bring S to a value < 0 ($> S_{max}$), S is automatically put to 0 (a spike is immediately generated). We emphasize the fact that spike latency enables a mechanisms to encode neural information, and is supported from all the most plausible models. Thus, there is lack of information in models that do not exhibit this relevant property.

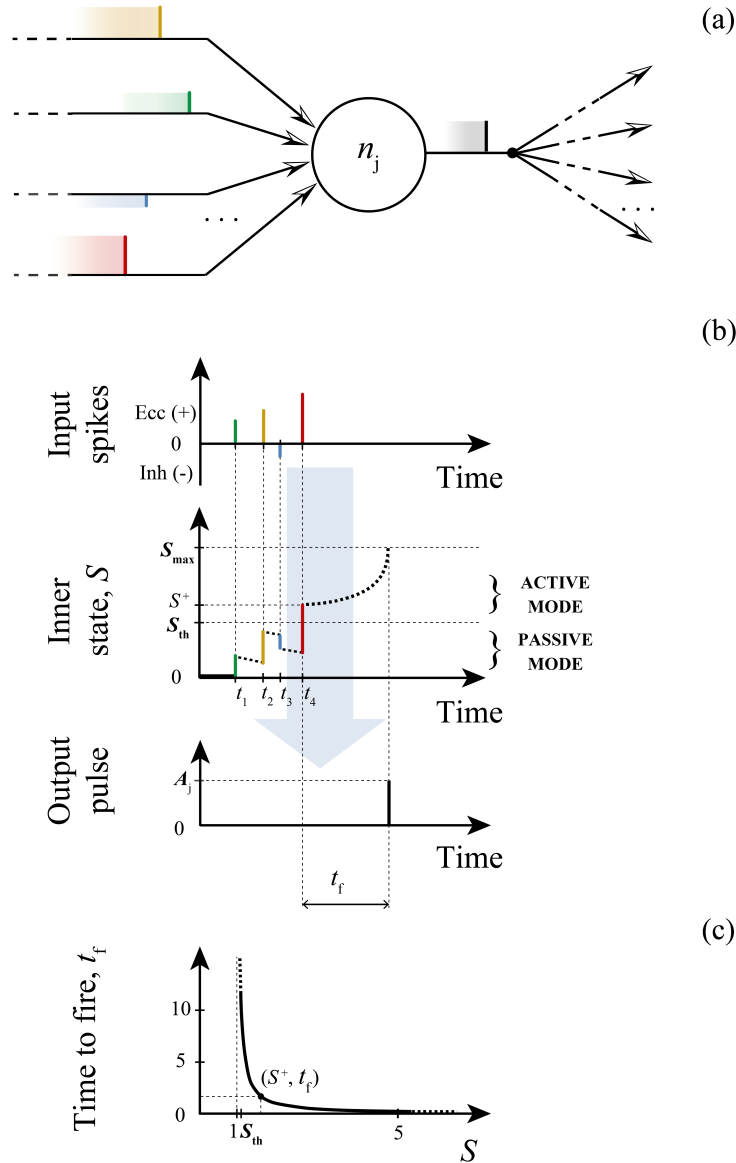


Figure 2. Neural summation and spike generation in a LIFL neuron. (a) Input/output process scheme; (b) temporal diagram of LIFL operation (basic configuration), assuming the neuron starts from its resting potential. Each incoming excitatory (inhibitory) input causes an instantaneous increase (decrease) of the inner state. In passive mode the neuron is affected by a decay; when S exceeds the threshold ($S = S^+$) the neuron is ready to spike; due to the latency effect, the firing is not instantaneous but it occurs after t_f . Once emitted, the pulse of amplitude A_j (equal to A_{exc} if the neuron j is excitatory as supposed to be in this case, without loss of generality) is routed to all the subsequent connections. In (c) is shown the firing equation, i.e., the latency curve for the determination of t_f from S^+ (see Salerno et al., 2011). The simplest case of firing equation curve has been chosen ($a = 1, b = 0$), and c set to 0.04

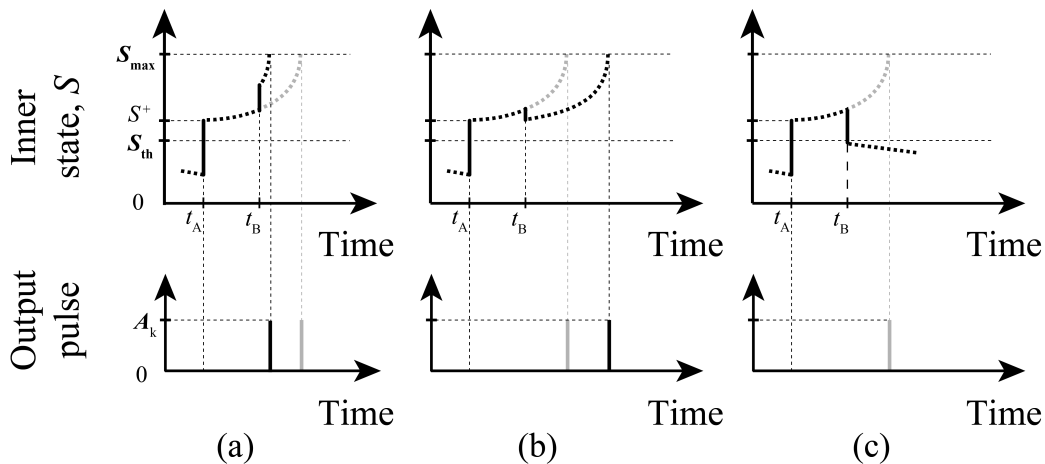


Figure 3. Arrival of further inputs when the neuron is overthreshold. (a) The arrival of a new excitatory synaptic pulse at time t_B anticipates the spike generation (post-trigger anticipation). The arrival of a new inhibitory synaptic pulse at time t_B is able to (b) delay the spike generation (post-trigger postponement), or (c) to cancel the spike generation (post-trigger inhibition). In order to simplify the comparison, the state evolution in active mode in the simple case of no further inputs is reported in the same figure (grey). Neuron k is supposed to be excitatory as in Fig. 2.

Hitherto we have discussed a basic configuration of LIFL, which defines an intrinsically *class 1 excitable, integrator* neuron, supporting *tonic spiking* and *spike latency*. Nevertheless, thanks to the “modularity” of its mathematical model, such neuron can be easily enriched with other neuro-computational features (see Izhikevich, 2004) by introducing minimal modifications to the model equations (see *Appendix B*).

Of course, it is possible to further improve the neuron model by adding extrinsic properties at the programming level. This is the case of the *refractory period*, already implemented in FNS, for which after the spike generation the neuron inner state remains set to zero for a period t_{arp} (set by the user), when the neuron becomes insensitive to further incoming spikes. The same strategy can be used for modelling other neurocomputational features and reproducing different kinds of cortical neurons (see *Appendix B*).

In addition to the temporal aspects emerging from the pure computation of the neuron (i.e., latency), in the next section another kind of delay will be introduced, independent from the activity, used to characterize the long-range connections between neurons belonging to different groups.

2.2. Connection between 2 neurons

FNS allows us to create brain models where regions are composed of neuron modules (i.e., network nodes). Neurons of the same node interact instantaneously, whereas a settable time delay (≥ 0) is present between neurons of different nodes. Such architecture reflects the actual communication between network nodes, that are spatially remote from each other (Maslennikov and Nekorkin, 2014).

Then, as general model of neuronal link, both *axonal lengths* and *synaptic weights* are taken into consideration. Such two link elements (belonging to a directed connection) are able to introduce both delay and amplification/attenuation of the passing pulse, respectively. A scheme of inter-node neuron connection ($e_{i,j}$) is illustrated in Fig. 4, where $\lambda_{i,j}$ represents the *axonal length* block, and $\omega_{i,j}$ the *synaptic weight* block. As in Nakagawa et al. (2014); Cabral et al. (2014) a global propagation speed v is set for FNS simulations, so that inter-node connection delays are automatically defined from the axonal lengths, as $\tau_{i,j} = \lambda_{i,j}/v$. Connection delays are important since they allow to take into account the three-dimensionality (i.e., spatial embeddedness) of the real anatomical brain networks. For the motivations mentioned before, conversely to the inter-node connection (represented as $e_{i,j}$ in Fig. 5), intra-node connection (represented as $e_{j,k}$ in Fig. 5) does not provide the axonal length block (although synaptic weight block continues to be defined).

For biological and mathematical reasons, it is desirable to keep the synaptic weights under a certain value, W_{max} , a global parameter of the model.

2.3. From brain regions to graph nodes

FNS allows us to define regions constituted by one or more *nodes* where each node consists of a neuron module with specific properties. In order to reproduce heterogeneous nodes, a Watts-Strogatz based generative procedure is implemented (Watts and Strogatz, 1998) as detailed below, allowing the generation of complex networks with structure properties of real neuron populations.

The implemented procedure allows us to model intra- and inter-node diversity: number of neurons and connectivity, percentage of inhibitory neurons, distribution of weights and type of neuron; in addition, the possibility to represent a region with more than one node permits to model intra-region neuronal pools of different connectivity and neuron types. In the extreme case, a module can be composed of a single neuron, e.g., for reproducing

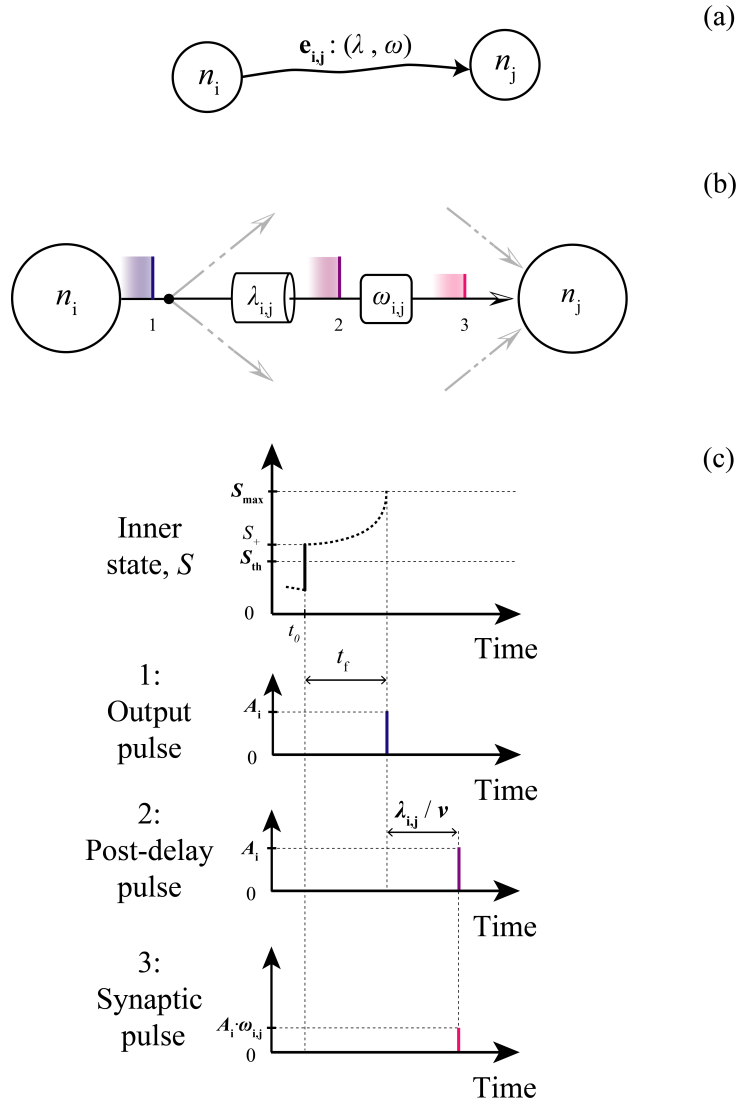


Figure 4. Neuron connection model and pulse transfer. (a) compact representation, (b) logical block representation, (c) temporal diagram: length block produces a translation of the output pulse along time axis whereas weight block is able to increment/decrement its amplitude. Note that in this example the neuron is supposed to be excitatory, otherwise all the amplitudes would be negative. Output pulses can be considered as a correlate of spiking activity, whereas synaptic pulses can be considered as correlate of synaptic currents

small and deterministic motifs. In the following sections such procedure is illustrated; after it will be explained how intra- and inter- node connections are made.

2.3.1. Watts-Strogatz-based module generation procedure

The original Watts-Strogatz procedure is able to generate different types of complex networks (from regular to random), including networks with *small-world* properties (i.e., networks that present large *clustering coefficient* and small *average path length*), that has been demonstrated to reasonably approximate a mid-sized patch of cortex (in the order of $10\mu m$) with its neighborhood (Riecke et al., 2007). The original Watts-Strogatz procedure is here adapted to generate a module including both inhibitory and excitatory, oriented, connections, analogously to (Maslennikov and Nekorkin, 2014). Given the integer n (i.e., *number of neurons*), k (i.e., *mean degree*), p (i.e., *rewiring probability*), and R (i.e., *excitatory ratio*), with $0 \leq p \leq 1$ and $n \gg k \gg \ln(n) \gg 1$, the model constructs an oriented graph with n vertices and nk single connections in the following way:

- a regular ring lattice of n spiking neurons is created, of which $R \cdot n$ are able to send excitatory connections and the remaining $(1 - R) \cdot n$ are able to send inhibitory connections;
- for each neuron an outgoing connection to the closest k neurons is generated ($k/2$ connections for each side, with k integer and even);
- for each neuron i , every link $e_{i,j}$ with $i < j$, is rewired with probability p ; rewiring is done by exchanging $e_{i,j}$ and $e_{i,m}$ where m is chosen with uniform probability from all possible (excitatory or inhibitory) neurons that avoid self-loops ($m \neq i$) and link duplication. This process is repeated n times, each one considering a different neuron.

Note that the p parameter allows to interpolate between a regular lattice ($p = 0$) and a random graph ($p = 1$): as p increases, the graph becomes increasingly disordered. For intermediate values of p the network presents small-world properties. The parameters n , k , p represent instruments to customize the network nodes on the basis of the real anatomy. For example, n can be chosen in accord to the volume of the region that is intended to be represented (estimated from a specific subject using available techniques, as in Bassett et al. (2008), or extracted from existing *atlases*).

2.3.2. Characterization of intra-module connections

Once connections have been established, weights have to be assigned. Several authors have addressed this problem, setting intra-node weights in different manners. Depending on the specific study, weights have been chosen to have the same, static value (Deco and Jirsa, 2012), or characterized by a specific distribution (Abuhassan et al., 2014), or varying in a certain range by means of plasticity (Izhikevich et al., 2004). In order to encompass the most of these possibilities, in FNS two sets of Gaussian distributed values can be defined by the user for the initialization of the intra-module weights of each module: one for the excitatory (defined by mean $\mu_{w_{exc}}$ and standard deviation $\sigma_{w_{exc}}$) and one for the inhibitory (defined by $\mu_{w_{inh}}$ and $\sigma_{w_{inh}}$) (see *Appendix C*). In addition, it is possible to enable STDP plasticity, with different parameters for each module, as we will show in Sect. 2.5.

2.4. From fibre tracts to graph edges

In FNS an *edge* represents a monodirectional set of long-range axons that links a module to another. In the brain, conversely to intra-node connections, inter-node connections are characterized by non negligible delays, which are determined by axon length, diameter and myelination.

2.4.1. Characterization of inter-region connections

Proper number of connections N_e and distributions of weights and lengths can be set for FNS edges. The distribution of edge weights follows a Gaussian function (as in Abuhassan et al., 2014), characterized by the parameters μ_ω and σ_ω . Differently, a gamma distribution is implemented for the edge lengths, characterized by mean parameter μ_λ and shape parameter α_λ (see *Appendix C*), since there is probably not a unique prototypical shape for edge delays (as discussed in Vicente et al., 2008). This allows the user to explore different shapes, to investigate the impact of different choices on the network activity, to mimic pathological states as the effect of structural inhomogeneity (as discussed in Ton et al., 2014), or spatially-selective conduction speed decrease due to demyelination (Smith, 1994).

Since in FNS inter-region connections are intended to represent those of pyramidal neurons, they are limited to act between excitatory neurons (as in Nakagawa et al., 2014; Maslennikov and Nekorkin, 2014), randomly chosen among those of the involved nodes, conversely to intra-node connections, that can exist between all types of neurons. See Fig.5 for details.

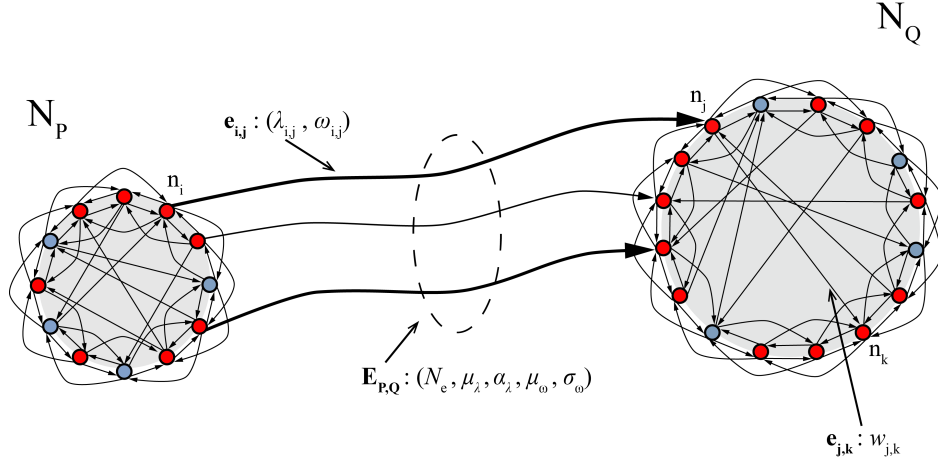


Figure 5. Two nodes connected by an edge. While an intra-node connection is characterized by its weight, an inter-node connection is defined by weight and length; an edge is defined by number of axons and related distribution of weights and lengths. Inter-node connections are established among neurons that send excitatory connections (red neurons) in their module, chosen randomly. In order to represent the two modules, for illustrative purpose the following values are used: $n_1 = 12$, $n_2 = 16$; $R_1 = 2/3$, $R_2 = 3/4$; $k_1 = k_2 = 4$; $p_1 = 1/6$, $p_2 = 1/8$.

2.5. STDP

Synaptic plasticity consists of an unsupervised spike-based process able to modify weights on the basis of the network activity. The STDP, a well-known type of plasticity mechanism, is believed to underlie learning and information storage in the brain, and refine neuronal circuits during brain development (Sjöström and Gerstner, 2010). Considering a synapse connecting two neurons, such mechanism is based on the precise timings of *presynaptic pulse* (i.e., the *synaptic pulse* arriving from the presynaptic neuron) and *postsynaptic pulse* (i.e., the *output pulse* generated by the postsynaptic neuron), influencing the magnitude and direction of change of the synaptic weight. In case of inter-node connection the presynaptic pulse is taken after the axonal delay block and not before, in order to avoid the loss of causality information due to the axonal delay. The original STDP behaviour Bi and Poo (1998) can be approximated by two exponential functions (Abbott and Nelson, 2000).

$$\Delta W = \begin{cases} A_+ e^{-\frac{\Delta T}{\tau_+}}, & \text{for } \Delta T > 0 & (6a) \\ 0, & \text{for } \Delta T = 0 & (6b) \\ A_- e^{\frac{\Delta T}{\tau_-}}, & \text{for } \Delta T < 0 & (6c) \end{cases}$$

where:

- ΔT is the difference between postsynaptic pulse generation (i.e., t_{post}) and presynaptic pulse arrival (i.e., t_{pre}) instants:

$$\Delta T = t_{post} - t_{pre} \quad (7)$$

as illustrated in Fig. 6

- τ_+ and τ_- are positive time constants for *long-term potentiation* (LTP, 6a) and *long-term depression* (LTD, 6c), respectively;
- A_+ and A_- are chosen in order to keep weight values bounded between minimum and maximum values (as discussed in Sect. 2.2).

Then, a weight is increased or decreased depending on the pulse order (*pre*-before *post*-, or *post*- before *pre*-, respectively). To make the weight change dependent also on the current weight value, *soft bounds* (Sjöström and Gerstner, 2010) are introduced in FNS, so that $A_+(W_p) = (W_{max} - W_p)\eta_+$ and $A_-(W_p) = W_p\eta_-$, where W_p is the past value of the synaptic weight, W_{max} the upper bound (see 2.2), and η_+ and η_- are learning constants, positive and usually relatively small ($\sim 10^{-5}$), since the learning process is on a much slower time scale than the neural dynamics (Kempster et al., 1999). The weight update relations implemented in FNS are:

$$W = \begin{cases} W_p + (W_{max} - W_p)\eta_+ e^{-\frac{\Delta T}{\tau_+}}, & \text{for } \Delta T \geq 0 & (8a) \\ W_p - W_p\eta_- e^{\frac{\Delta T}{\tau_-}}, & \text{for } \Delta T < 0 & (8b) \end{cases}$$

It is important to stress that the *soft-bounds* approach allows an increase of both the synaptic capacity and the memory lifetime, in respect to the alternative *hard-bounds* approach (van Rossum et al., 2012).

In addition, to make STDP event list management costless, exponential tails are suppressed after a certain time value $TO \cdot \max(\tau_+, \tau_-)$, where TO is

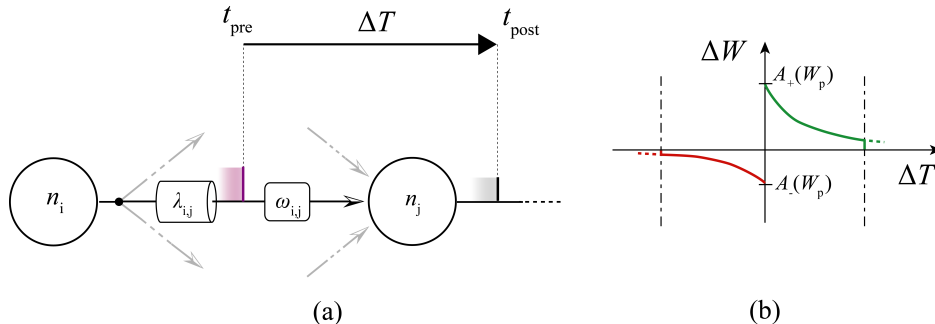


Figure 6. STDP process in FNS: (a) ΔT calculation in relation to the synapse w_{ij} , considering an inter-module connection (without loss of generality); (b) Shapes of the learning windows (LTP in green, LTD in red) considering exponential tail suppression (dash dot).

the *STDP timeout constant*, defined by the user. In this way, burning-firing couples whose interval exceeds such time limit are not considered for the STDP process (see Fig. 6). Learning windows are typically in the order of 100 ms.

STDP varies tremendously across synapse types and brain regions (Abbott and Nelson, 2000; Caporale and Dan, 2008)

In order to contemplate inter-node synapse diversity, in FNS, is possible to specify a different set of STDP parameters for each node, or to selectively apply STDP only for certain nodes.

2.6. Input stimuli

Several types of stimuli can be of interest in brain simulation studies. Of these, two prototypical types of stimuli are:

- the noisy fluctuations typically observed in vivo, which can be modeled by uncorrelated Poisson-distributed spike trains (see Frohlich et al., 2008; Abuhassan et al., 2014; Nakagawa et al., 2014);
- the DC current used by neurophysiologists to test some neuron features (Izhikevich, 2004) that can be modeled by constant spike trains (as in Vicente et al., 2008).

In addition, in many simulation scenarios the possibility of giving arbitrary spike streams (e.g., sequences that mimic sensory-like processed data) can be of interest, in order to test the response of specific subnetworks.

In light of what has been discussed, in FNS it is possible to stimulate brain nodes with these three different types of inputs. The user is allowed to stimulate all or only a part of the network nodes, choosing the kind of input to inject to each one of them. Input pulses are assumed to be all excitatory.

2.6.1. Poisson-distributed spike train

This option provides the injection of spike trains distributed according to an homogeneous Poisson process, in which the underlying *instantaneous firing rate* r_P (Gerstner et al., 2014), is constant over time.

Given a long interval (t_A, t_B) we place a single spike in that interval at random. Then, considering the sub-interval (t_1, t_2) of length $\Delta t = t_2 - t_1$, the probability that the spike occurs during this sub-interval is equal to $\Delta t / (t_B - t_A)$. Now, placing k spikes in the long interval, the probability that n of them fall in the sub-interval is given by the following binomial formula:

$$P\{n \text{ spikes during } \Delta t\} = \frac{k!}{(k-n)!n!} p^n q^{k-n} \quad (9)$$

where $p = \delta t / (t_B - t_A)$ and $q = 1 - p$.

Under proper conditions this expression can be rewritten removing the time dependence as:

$$P\{1 \text{ spike during } \delta t\} \approx r \delta t \quad (10)$$

This equation can be used to generate a Poisson spike train by first subdividing time into a set of short intervals, each one of duration δt . Then generate a sequence of random numbers \mathbf{R} , uniformly distributed between 0 and 1. For each interval i , a spike is generated if $\mathbf{R}(i) \leq r \delta t$. This procedure is appropriate only when δt is very small, i.e, only when $r \delta t \ll 1$ (Heeger and Heeger, 2000).

In FNS, a user-defined number of fictive *external neurons* $n_{extP,k}$ is set for each stimulated node N_k . By defining a $t_{startP,k}$ and a $t_{endP,k}$ for the external stimuli, each external neuron can send spikes in a discrete number of instants $(t_{startP,k} - t_{endP,k}) / \delta t_P$. The target neurons receive pulses of amplitude $A_{P,k}$.

Pulses are injected from each external neuron to all neurons belonging to a set of nodes defined by the user, by specifying the following set of parameters for each chosen node N_k : $n_{extP,k}$, $t_{startP,k}$, $t_{endP,k}$, $r_{P,k}$, $\delta t_{P,k}$ and $A_{P,k}$.

2.6.2. Constant spike train

This option provides the injection of constant spike trains in order to emulate DC current stimulation. Note that since we simulate the network by means of an event-driven approach, the *DC* input is not continuous as in the real counterpart, but it is constantly sampled with an adequately small time step (i.e., smaller than the spike duration) called *interspike interval* and indicated with int_c .

In FNS, a user-defined number of fictive *external neurons* $n_{ext,c,k}$ is set for each stimulated node N_k . Each external neuron can send spikes from time $t_{start,c,k}$ to $t_{end,c,k}$, with amplitude $A_{c,k}$. Such kind of input is injected from each external neuron to all neurons belonging to a set of nodes defined by the user, by specifying the following set of parameters for each chosen node N_k : $n_{ext,c,k}$, $t_{start,c,k}$, $t_{end,c,k}$, $int_{c,k}$ and $A_{c,k}$.

Note that the situation $int_{c,k} < t_{arp,k}$ should be avoided because pulses would arrive during the refractory time.

2.6.3. Arbitrary spike stream

Arbitrary spike streams can be injected to neurons belonging to a set of nodes defined by the user by specifying the following set of parameters for each chosen node N_k : the spike *amplitude* $A_{ss,k}$, and a couple $(n_{ss,k}, t_{ss,k})$ for each event to introduce (i.e., *external source number* and related *spike timing*, respectively). External sources are permanently associated to the neurons of the indicated node, using a random procedure.

2.7. Output signals

Depending on the type of contributions we are considering at the network level, i.e., output pulses (corresponding to *action potentials*) or synaptic pulses (corresponding to *postsynaptic currents*), the same network activity gives rise to different signals, due to the presence of delays and weights in the model.

In particular, action potentials coincide with the activity emerging from *firing* events (see Sect. 2.1.2), because they take place before the axon, thus they are spatially localized at the transmitter node; whereas postsynaptic currents coincide with the *burning* activity (see Sect. 2.1.2), because they take place downstream the axon, thus they are spatially localized to the receiver node, and are affected by the shifting effect introduced by (heterogeneous) fibre tract's delays and synaptic weights.

Action potentials are of interest for some studies (see Vicente et al., 2008), whereas postsynaptic currents can be useful for some others (see Mazzoni et al. (2008); Nakagawa et al. (2014) for LFP and MEG signal reconstruction).

In order to give the user the possibility to reconstruct such different types of signals, output section of FNS allows to store both firing and burning times (t_F and t_B), transmitter and receiver neurons (n_F and n_B) and related nodes (N_F and N_B), as well as amplitude weights (W_{ev}) involved in each event occurring during the simulation interval, for some nodes indicated by the user before the simulation starts.

3. Simulation framework structure

On the basis of the modelling introduced in the previous section, here we describe the framework structure and the tools it offers to the user for implementing a brain network, stimulating it, and obtaining the outputs of interest.

The framework is articulated in three main sections (see Fig. 7): *Generator section*, *Neuroanatomical model section* and *Output section*, which can be programmed by the user by means of proper *vectors* (whose internal software representation is illustrated in Sect. 4.1). Referring to the parameters introduced during the paper, such vectors are defined in table 1, represented in Fig. 7 and explained in the following paragraphs.

Section	Vector/Set	Components	Name	
Generator section	PV	n_{extP}	number of <i>Poisson spike train</i> external neurons	
		t_{startP}	Poisson input onset	
		t_{endP}	Poisson input offset	
		r_P	firing rate	
		δt_P	delta	
	CV	n_{extc}	number of <i>constant spike train</i> external neurons	
		t_{startc}	constant input onset	
		t_{endc}	constant input offset	
		int_c	interspike interval	
		A_c	constant input amplitude	
	SV	t_{ss1}, t_{ss2}, \dots	<i>input stream</i> spike timings	
		n_{ss1}, n_{ss2}, \dots	related neuron numbers	
		A_{ss}	stream input amplitude	
	Neuroanatomical module section	LDV	n	number of neurons
p			rewiring probability	
k			mean degree	
R			excitatory ratio	
μ_{wexc}			intra-node excitatory weight distr.mean (Gaussian)	
σ_{wexc}			intra-node excitatory weight distr.st.dev. (Gaussian)	
μ_{winh}			intra-node inhibitory weight distr.mean (Gaussian)	
σ_{winh}			intra-node inhibitory weight distr.st.dev. (Gaussian)	
a			latency curve center distance	
b			latency curve x-axis intersection	
c			threshold constant	
D			decay parameter	
t_{arp}			absolute refractory period	
ICV			N_e	number of connections (edge cardinality)
		μ_ω	inter-node weight distr.mean (Gaussian)	
		σ_ω	inter-node weight distr.st.dev. (Gaussian)	
		μ_λ	inter-node length distr.mean (gamma)	
		α_λ	inter-node length distr.shape (gamma)	
		STDPV	τ_+	LTP time constant
τ_-			LTD time constant	
η_+			LTP learning constant	
η_-			LTD learning constant	
GPV		A_{exc}	excitatory presynaptic amplitude	
		A_{inh}	inhibitory presynaptic amplitude	
		W_{max}	maximum weight	
		TO	STDP timeout constant	
		v	global conduction speed	
		t_{stop}	simulation stop time	
Output section		NV	NOI_1, NOI_2, \dots	list of <i>NOIs</i>
		FV	n_F	firing neuron number (if firing event)
			N_F	firing node number (if firing event)
			t_F	firing event time (if firing event)
		BV	n_B	burning neuron number (if burning event)
	N_B		burning node number (if burning event)	
	t_B		burning event time (if burning event)	
	W_B		synaptic weight (if burning event)	

Table 1. Definition of the system parameters.

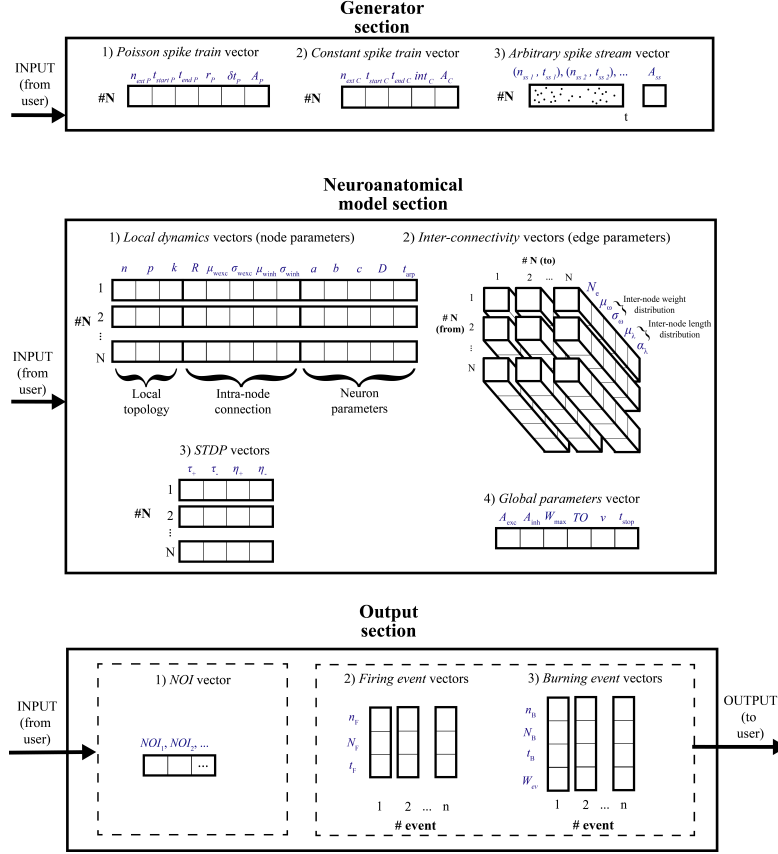


Figure 7. FNS framework overall structure.

3.1. Generator section

This section allows the user to inject the desired input to some selected nodes. *Poisson spike train vectors* (i.e., **PV**), *constant spike train vectors* (i.e., **CV**) and *arbitrary spike stream vectors* (i.e., **SV**) can be combined to send more than a kind of input to the same node simultaneously.

3.2. Neuroanatomical model section

Neuroanatomical model section allows the user to define the network model: local dynamics, structural parameters, plasticity constants and global parameters. Each node is fully characterized by a *local dynamics vector* (i.e., **LDV**), where the subset $[n, p, k]$ defines the *local topology*, the subset $[R, \mu_{wexc}, \sigma_{wexc}, \mu_{winh}, \sigma_{winh}]$ defines the *intra-node connection parameters* and the subset $[a, b, c, D, t_{arp}]$ defines the *neuron parameters*; as stressed in

Sect. 2.2, connection delay is absent in intra-node connections. From the definition of node’s weight distribution, the simulator computes all the single intra-node synaptic weights and stores them in proper data structures (see Sect. 4.1).

Each edge is fully characterized by a *inter-connectivity vector* (i.e., **ICV**), where $[N_e]$ defines the *edge cardinality*, the subset $[\mu_\omega, \sigma_\omega]$ defines the *inter-node weight distribution* and $[\mu_\lambda, \alpha_\lambda]$ defines the *length distribution parameters*. From the definition of such parameters the simulator computes all the single inter-node lengths and weights and stores them in proper data structures (see Sect. 4.1).

Note that values arising from both intra-node weights and inter-node lengths distributions have to be positive to be stored in the internal matrices; in case they assume negative values FNS allows the user to consider the absolute value of such quantities, or to terminate the program execution. In addition, weight values don’t have to exceed the value W_{max} .

The *STDP vector* (i.e., **STDPV**) defines the STDP to act on a specific node. Such vector contains all STDP parameters discussed, except *TO* that is a global parameter.

The global parameters of the system are defined by the *global parameters vector* (i.e., **GPV**). Among these, t_{stop} specifies the neural activity time we want to simulate in biological time units (*ms* in our case).

3.3. Output section

Output section allows the user to choose regions and type of contributions for which to obtain information. Before the simulation starts, the user can specify the list of nodes for which to store all simulation data (*nodes of interests*, or NOIs) through the *NOI vector* (i.e., **NV**). At the end of the simulation, data of all firing and burning events in which such NOIs are implicated are available to the user, in form of a vector for each event. Depending whether it is a firing or burning event, in the output we obtain different vectors: *firing event vector* (i.e., **FV**) and *burning event vector* (i.e., **BV**), respectively.

4. Implementation aspects

FNS runs in two phases: the first phase consists in the initialisation of the data structures needed by the simulation; the second phase consists in the simulation of events.

The first phase is made by a set of sequential steps:

- reading of *Generator section* and *Neuroanatomical model section* configuration vectors, and specification of the NOIs for which the event vectors FV and BV (of *Output section*) have to be stored;
- creation of node-specific data structures and neuron clusters to be run concurrently;
- creation of global data structures;
- initialization of the whole simulator run.

After those steps have been accomplished, the simulation phase begins. The parallelization strategy implemented allows the program to proceed through the simulation of single slices of simulated time, with a specific and constant duration, for multiple nodes at the same time. Each cycle terminates with the synchronization between node sets whose events affects each other; then, the simulation proceeds with the next cycle, and so on.

4.1. Data structures

Once parameters have been entered from the user, the program proceeds to initialise single values of weight and delay. If there are values arising from the distributions that violate *distribution values bounds* introduced in Sect. 3.2, the user can choose between rectify them or terminate the program execution. Below we briefly describe the main data structures used by the software, highlighting which of these act at the node level:

connection object: it emulates a generic biological axon with associated synapse, specifying *length*, *weight*, connecting a *firing* neuron to a *burning* one;

inter-connection dictionary: map where each entry represents a couple (weight, length) of an inter-node connection linking the firing neuron of a node A to the burning neuron of a node B ($B \neq A$). Weights are defined from a Gaussian distribution whose parameters μ_ω (i.e., the mean value) and σ_ω (i.e., the standard deviation) are specified by the user for each couple of network nodes; lengths are defined from a gamma distribution whose parameters μ_λ (i.e., the mean parameter) and α_λ (i.e., the shape parameter) are specified by the user for each couple of network nodes;

intra-connection dictionary (node-specific): this is the intra-node equivalent of the *inter-connection* dictionary, where each entry represents the weight of an intra-node connection. Such weights are defined from a Gaussian distribution which parameters μ_w (i.e., the mean value) and σ_w (i.e., the standard deviation) are specified by the user for each network node;

state dictionary (node-specific): it contains the inner states of the neurons pertaining to a specific node, and it is constantly updated through the node simulation;

active neurons list (node-specific): list of active neurons pertaining to a specific node, sorted on their firing time; this list is constantly updated through the node simulation;

outgoing spike list (node-specific): lists of output pulses, including burning neuron, node and instant, generated from a specific (firing) node within a specific time slice;

STDP timing list: it temporarily stores event timings in order to compute the ΔW . The latter are automatically discarded after the TO value defined by the user.

4.2. Event-driven procedure

In an asynchronous or event-driven algorithm, the simulation advances from an event to the next one. As stressed in Sect. 1, such asynchronous computation of events makes it possible the simulation of very large networks by quite simple computing procedures. In the simple case of no latency and identical transmission delays, the data structure for the queue can be just a FIFO (*First In, First Out*) queue, which has fast implementations (Cormen et al., 2001). In FNS, a more complex procedure and data structures (as shown in Sect. 4.1) are needed to achieve this task.

The procedure is based on the list of firing events. In any instant, each network neuron is characterized by its inner state; each active neuron is also characterized by its proper t_f . When a firing event occurs, it propagates toward target neurons taking into account connection delays (if present). Such events modify the inner state of burning neurons (and their t_f , for active neurons), on the basis of the amplitude and sign of the pulse, and the time elapsed from the last state update. Four different cases of state update can happen to the target neuron:

- *passive-to-passive*. This does not have any effect on the event list
- *passive-to-active*. This elicits the insertion of an event (and related firing time) orderly on the event list
- *active-to-active* (i.e., post-trigger anticipation/postponement). This elicits the update (and reordering) of its firing time on the event list
- *active-to-passive* (i.e., post-trigger inhibition). This elicits the elimination of an event (and related firing time) from the event list

In addition to the four cases listed, two “forbidden” cases can occur during the simulation: from *passive mode* to $S < 0$ and from *active mode* to $S \geq S_{max}$; for such cases, specific actions are included in the procedure (state value instantaneous correction and output spike production, respectively).

4.3. Parallelization

4.3.1. Parallelization in event-driven simulators

In the parallel computing scenario the problem needs to be splitted in many sub-problems such that their solutions can be computed independently and then collected to provide the global solution. When using parallel processing units, one has to ensure that events are processed in the correct time order, but in brain simulation it is not trivial to determine which events can be executed in parallel because of the interdependence (cause-effect relations) between network elements (D’Haene, 2006; Grassmann and Anlauf, 1998). This introduces the need for synchronization mechanisms to keep different subsimulators synchronized to execute in the correct event chronological order, avoiding causality errors (D’Haene, 2006).

Many attempts have been made in last years to parallelize event-driven SNNs (e.g. Mouraud and Puzenat, 2009; D’Haene, 2006; Lobb et al., 2005; Grassmann and Anlauf, 1998; Djurfeldt et al., 2005; Delorme and Thorpe, 2003). FNS uses an *ad-hoc* parallelization strategy to accomplish this task: on the one hand, no event is leaked in order to speed up the synchronization of the parallel simulations. On the other hand, the algorithm adaptively chooses an appropriate interval of simulated time to adopt for the synchronization of the parallel tasks avoiding as much as possible the underuse of available hardware resources. Referring to the categorisation of D’Haene (2006) FNS implements an “adaptive” event-driven parallelization method.

4.3.2. Parallelization in FNS: the Bounded Opaque Period

Given a generic network, the *opaque period* (OP) is the minimum simulated time needed by a signal to travel from a network element to an adjacent one (Lubachevsky, 1989). Then, within any simulated time window smaller than the OP of the network, each (firing or burning) event cannot be caused by (or cannot affect to) any other event arisen in the same time window. In other words, if the time distance between the occurrences of two events is strictly less than the OP, those events have to be considered unrelated in terms of cause-effect relation; then, naming B the network OP, given the *time slice* T_s , with:

$$T_s < OP \quad (11)$$

we can compute each event independently to the others that are occurring in the same interval. This allows us to parallelize the computation within T_s . In formulas, we have:

$$0 \leq B < +\infty \quad (12)$$

and ev_1 and ev_2 are two distinct events such as

$$|\tau(ev_j) - \tau(ev_i)| < B, \quad i \neq j \quad (13)$$

then they can be computed in parallel without loss of cause-effect relationship (*Bounded Lag restriction*) (Lubachevsky, 1989). On the other hand, such parallelization could be performed only in a time window smaller than the *OP*: each unit must wait until each of the other has ended to simulate the events of the same specific T_s ; then, a *sync step* is needed to "deliver" the events just calculated to the unit which should use them to produce new events during the next *OPs*.

Unfortunately, in the case of neural network a huge amount of events can occur in a short time interval, thus an event could affect another one in a very short time; the short OPs (i.e., the high synch steps frequency) counteract the benefit of the parallelization, making the parallel approach worse than the sequential one. To overcome those difficulties, the Lubachevsky's idea has been properly adapted to fit our problem:

while intra-node interactions are instantaneous (i.e., firing and burning coincide then it is not possible to compute them in parallel), inter-node

interactions generally are not, then a certain simulated time > 0 is needed by a neuron of a node to affect the state of a neuron of another node. At most, if a number of nodes of the network are inter-connected without inter-node delay, we can consider such nodes as a single one, and the statement continues to be valid. We define *bounded opaque period* (BOP) the minimum among all the network inter-*group* connection delays, where for *group* we intend a single node, or a set of nodes inter-connected with zero-delay (if present in the network).

The fact of considering the more ample concept of group instead that of node in some simulation steps, enables the possibility of representing heterogeneous regions without losing the parallelization feature (see Sect. 2.3). As the OP, the BOP is a network value.

Let U and V be two distinct groups of the network, and u and v two neurons respectively belonging to groups U and V ; for the BOP \bar{B} it is true the following:

$$\begin{aligned} ev_{u,i} \rightarrow ev_{v,j} \Rightarrow \tau(ev_{v,j}) - \tau(ev_{u,i}) \geq \bar{B}, \quad \forall u \in U \\ \forall v \in V \\ U \neq V \end{aligned} \tag{14}$$

where the single arrow means that the (firing) event $ev_{u,i}$ generated by the neuron u , affects the inner state of the neuron v , generating the (burning) event $ev_{v,j}$. As corollary we have that given two events $ev_{u,i}$ and $ev_{v,j}$ for which holds the following:

$$\begin{aligned} |\tau(ev_{v,j}) - \tau(ev_{u,i})| < \bar{B}, \quad \forall u \in U \\ \forall v \in V \\ U \neq V \end{aligned} \tag{15}$$

they can be considered unrelated in terms of cause-effect relationship, thus they can be computed in parallel.

Each *thread* could be exclusively in the states *running*, *waiting* or *completed*. Each *thread worker* (i.e., CPU, GPU, etc.) can execute at most a thread at a time. In order to minimize processing times, each worker can serve queued threads in turns for a short time, and different workers can swap threads each other.

If we assign each group to a specific thread, we can execute the neuronal activity of each group without the need to care about the new inter-node spikes. If a thread generates a spike which has to be delivered to another group, it saves this spike to the node-specific *outgoing spike list*. The synch step provides the spike events in queue to be sent to right destination threads. Once a thread gets a spike event from a node, it puts this event orderly to the internal node-specific *active neurons list* and updates the burning neuron internal state at the right time.

Once **ICVs** (and then, the groups) have been defined, we can simulate the generation of events within each group using a specific thread. When the whole simulation starts, the steps until the completion of the execution are the following:

1. all threads are set as *runnable*;
2. each of them simulates the generation of events within the (simulated) BOP_1 (i.e., the time window from time $t = 0$ to time $t = \bar{B}$). If empty threads occur, for them the simulation jumps directly to point 3;
3. once a thread has generated all the events within the current BOP_1 window, it sets its status to *waiting*;
4. once all threads have completed to simulate the events of the BOP_1 window, all threads synchronize each other by delivering inter-node events to the corresponding threads (synch step) ;
5. all threads get again to the state *runnable* and simulate the events generated within the BOP_2 (i.e., the time window from time $t = \bar{B}$ to time $t = 2\bar{B}$), and so on.

This algorithm cycles until the triggering of some custom stop conditions (which can be set, e.g., on the overall simulated time, or on the cycle numbers, etc.).

Obviously, a firing event generated within BOP_n not necessarily will be delivered as burning event during BOP_{n+1} : it could be delivered in one of the following BOPs, depending on the connection delay involved.

The concept of parallelization through BOP is summarized in Fig. 8, where for simplicity we consider the simple *resonance pair* motif (Gollo et al., 2014; Maslennikov and Nekorkin, 2014) (i.e., two nodes bidirectionally connected with delay).

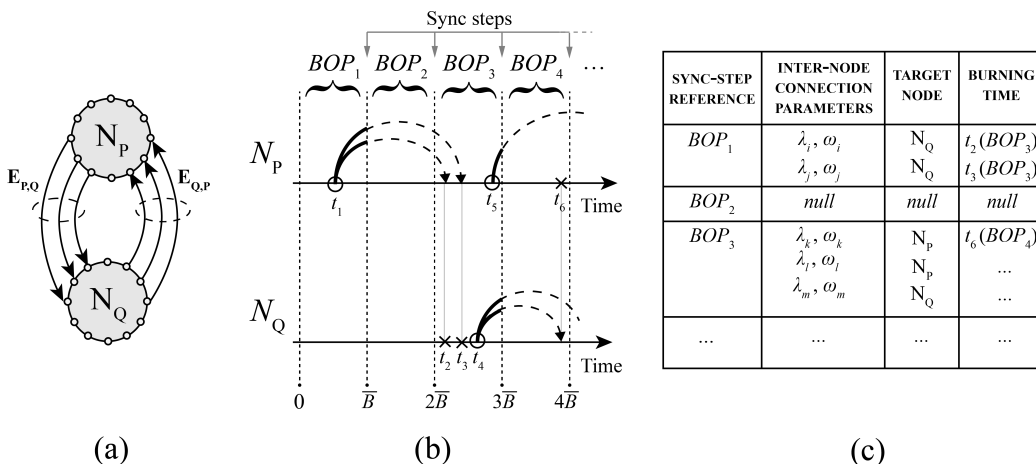


Figure 8. BOP-based parallelization mechanism. (a) Example network: two interconnected nodes are generating spiking activity (under proper external stimulation, not shown in the figure). (b) Temporal diagram of the parallelization process. Inter-node pulses are represented by dashed arrows, firing events by circles, burning events by crosses. An inter-node firing event generates burning events in the target node. The delivery of the events to the burning node will happen at the end of the firing event’s BOP. Given a firing event, related burnings will happen in one (or more) following BOPs. Given a burning event, the related firing event belongs to a BOP that precedes the current one (not necessarily the previous one). The axis represents simulated time. (c) Event schedule grid.

In *Appendix D* we report a simplified description (in pseudo-code) of the procedure implemented in FNS, supporting the synchronization mechanism between nodes.

Although a similar concept of “*Safe Window*” of simulated time has been used by Grassmann and Anlauf (1998), our work is oriented to a flexible multi-thread parallelization strategy (allowing the use also in threads configurations with shared memory as *CPUs* and *GPUs*), and not only to a distributed computing oriented technique. Our strategy disregards the way threads are assigned to workers; therefore they can be *CPU*, *GPU*, *MapReduce Tasks*, etc.

4.4. Why Java[®]?

FNS has been implemented using the general purpose open source programming language Java[®]. The big quantity of open source libraries available and the possibility to be run on almost any architecture, meet both the needs of trustworthiness and flexibility. Thanks to the *Java Garbage Collector*, we can focus on the optimization of the algorithms resources consumption without worrying about the best timing for releasing the unused memory. The latest Java versions are being enhanced with additional support for parallel computation and new parallelization features (Ponge, 2011), which we can exploit in the future to enhance the parallelism of our algorithms. The parallelization is currently implemented as a *multi-threaded* Java standalone application. Our next step is to translate our algorithm to the *CUDA* paradigm, to allow the parallel computing of FNS over GPU or *MapReduce paradigm* through, respectively, the *jcuda* and the *Apache Hadoop frameworks*.

5. Reproduction of spontaneous MEG functional connectivity

In order to reproduce subject specific brain’s spontaneous electrophysiological activity using FNS, both structural and functional connectomes have been extracted from a healthy participant using DTI and source-space MEG, respectively. Connectomes have been estimated using 14 regions (7 regions per hemisphere, see table 2) composing the Default Mode Network (Raichle et al., 2001; de Pasquale et al., 2010), a *task-negative* resting state network, which is more strongly active during idling states than during task performance. The participant’s structural connectivity was used to estimate a structural model in the simulator, and its functional connectivity was employed to fine-tune phase and model evaluation.

5.1. Simulation setup

For the simulation we used brain data of a 66 years old male, chosen by lot from the set of control participants of a previous study (Garces et al., 2014).

#	Name
1	Left precuneus
2	Right precuneus
3	Left isthmuscingulate
4	Right isthmuscingulate
5	Left inferiorparietal
6	Right inferiorparietal
7	Left superiorfrontal
8	Right superiorfrontal
9	Left middletemporal
10	Right middletemporal
11	Left anteriorcingulate
12	Right anteriorcingulate
13	Left hippocampus
14	Right hippocampus

Table 2. Description of the 7 NOI per hemisphere considered for the connectomes, obtained from the *Freesurfer* (Fischl, 2012) cortical parcellation in 66 regions (Desikan et al., 2006) such as in (Hagmann et al., 2008).

To model spontaneous activity, we adjusted LIFL unit parameters in order to emulate the behavior of pyramidal neurons: $a = 1$, $b = 0$, $c = 0.04$, $D = 0.07$, $t_{arp} = 2$.

An external excitatory background input is predisposed consisting of spike trains representing the noisy fluctuations observed in vivo, with amplitude chosen in such a way that an isolated neuron displays predominant spiking activity in the alpha band (i.e., 7.5-12 Hz), i.e. the frequency range that characterizes real resting state data (Abuhassan et al., 2014). Each node is modeled with $n = 100$ neurons for a total of 1400 neurons. $R = 0.8$ as revealed by experimental observations (Izhikevich et al., 2004) and $p = 0.5$ in order to obtain small-world properties. Remaining intra-node connectivity parameters are chosen in such a way that the postsynaptic activity of the nodes preserves its peak in the alpha band, ensuring in the meantime that there is no strict periodicity of individual oscillations, and under the condition $n \gg k \gg \ln(n) \gg 1$ (as discussed in 2.3.1), obtaining $k = 30$ and $\mu_{w_{e,i}} = 0.04$. Each edge is initialized with a number of connections $N_e/N_{e,max}$ between the considered brain regions, where N_e is equal to the number of streamlines connecting two NOIs reconstructed with DTI (see Garces et al., 2014, for the method) and the denominator operates the normalization of the values in the range $[0, 1]$. Distances between regions μ_λ have been initially set from the Hagmann DSI data set (Hagmann et al., 2008), available as a package of *The Virtual Brain* repository (Sanz Leon et al., 2013); for the

edges for which DTI detected fibres but no value is present in the Hagmann dataset template, we used the Euclidean distances between the centres of gravity of the regions. Final structural model counts 45000 connections, for which plasticity is deactivated since we are reproducing a static scenario. Simulations have been repeated with two free parameters with the goal to match the resulting FC profile with the real MEG data: conduction velocity v , which has been varied in the neighborhood of the best-matching value reported in literature (i.e., 5.1 m/s, see Cabral et al., 2014; Nakagawa et al., 2014), and interconnection weights μ_ω , which we varied in a range that ensures interaction between the nodes but without altering significantly the power spectrum previously set (i.e., [0.04, 0.07]). To extract a source-space MEG comparable signal from the model, the *burning event vector* is subsequently imported in Matlab where the events are collected in contiguous bins of 1 ms of simulated time, and the simulated time-series are calculated by summing up all synaptic pulses, as in Nakagawa et al. (2014).

From the simulated activity, for each combination of v and ω we discarded initial transients and extracted 5 segments of 4s of activity. Then we processed the trials of simulated activity in the same way of real MEG source space signal, with the method described in (Garces et al., 2014).

Finally, for both simulated and real signal we calculated the *amplitude envelope correlation* FC index (Brookes et al., 2011) between all pairs of nodes considered.

The comparison between MEG and model FC matrices is calculated through the Pearson’s correlation coefficient r between the strictly upper triangular parts of alpha band FC values across all links connecting the 14 regions of interest (as in Cabral et al. (2014); Nakagawa et al. (2014)), after the application of the Fisher-Z transform to the FC measures, due to the non-additivity of correlation coefficients (Zimmerman et al., 2003).

The model shows the best agreement with experimental data for $\omega = 0.055$, $v = 5.0$, reaching an average correlation of $r = 0.43$ between empirical and simulated FC profiles.

We have repeated the comparison between MEG and model FC after orthogonalizing the time series of MEG signal (before deriving their power envelopes, as described in Hipp et al., 2012) in order to remove any zero-lag correlations between the neural oscillatory processes. As in Finger et al. (2016), we find interestingly a worse model fit if zero-lag components are discarded in the whole empirical functional connectome, indicating that a considerable amount of functionally relevant synchrony takes place at zero-

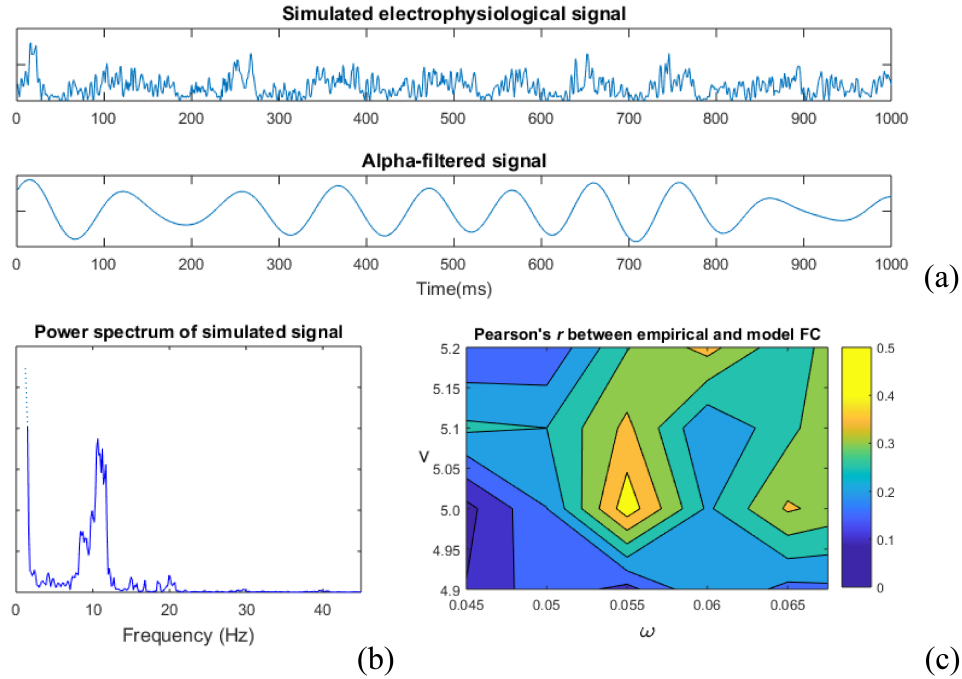


Figure 9. One second of simulated electrophysiological postsynaptic signal extracted from one node of the model with related alpha-filtered counterpart (a); power spectrum obtained from one of the trials (b); (c) represents the Pearson correlation coefficient between the simulated and the empirical FC as a function of simulation parameters v and ω

or near zero-lag.

In this example, for the reproduction of such signals we have done two major simplifications:

- the resulting signal more directly corresponds to a simulated LFP then to MEG. Nevertheless, a good correspondence between them has been reported (Nakagawa et al., 2014; Zhu et al., 2009) due to the fact that both signals arise from the same process (i.e., postsynaptic currents) (Buzsaki et al., 2012; Susi et al., 2018, under review);

- regarding the spatial organization of cortical neurons, we consider that pyramidal cells contribute the most to signal generation, taking into account that it is sufficient to reproduce the postsynaptic currents correctly, as shown in previous work (see Mazzoni et al., 2008, for an in-depth discussion on these aspects).

Although the aim of this section is to illustrate how a simulation can

be carried out in FNS, without a focus on the realism of the model, the comparison shows that the model is successful in reproducing the FC strength measured in real resting state MEG data.

FNS offers many possibilities for improving the model in order to achieve a better comparison with real data:

- simulate the whole-brain connectivity instead of focusing in the regions of a single resting state network. Some of the nodes of the presented network can, in the real case, be influenced by other nodes not included in this reduced model;
- model the brain with a higher parcellation resolution, increasing the number of nodes then employing a more heterogenous set of distances;
- implement diversity at different levels of the network, e.g. node-specific parameters (as differentiated number and type of neurons and intra-node weight distribution) and edge-specific parameters (as inter-node weights and delay distributions estimated from DTI, and presence of lateral connections);

It is important to note that the similarity between simulated and empirical FC strength could be underestimated due to limitations inherent to the quantification of FC from MEG data. In this work we have employed a linearly constrained minimum variance beamformer (Van Veen et al., 1997) for the resolution of the MEG inverse problem, which has been proven successful in the study of MEG resting state FC (Brookes et al., 2012; Hipp et al., 2012). However, other inverse solutions could be less sensitive to spatial leakage, such as the nulling beamformer (Hui et al., 2010). Finally, considering younger instead of middle-aged participants should result in a more accurate dynamics reproduction thanks to the better myelination state and axonal integrity (Branzoli et al., 2016).

5.2. Performance

Considering the example described above, the average time needed for generating a segment of 4 seconds of simulated activity is about 20 seconds of real time on an *Intel(R) Core(TM) i7-7700CPU @ 3.60GHz* (ram 16GB). The time needed for the initialization phase is about 2s; the remaining time is for the simulation phase. While the duration of the first phase depends on the network size only (number of neurons and connections of the network),

the duration of the second phase also depends on the value of minimum inter-node length of the network. This time can be reduced by increasing the *maximum heap size* in Java (set to 8GB in these simulations). If the user wants to re-execute the same experiment many times using the same topology data structures, there is no need to re-build it. In this case, the time needed to perform the first phase would be quite less, since the data structures image files will be reloaded. After the simulation FNS transcribes **FV** and **BV** of the selected NOI on two CSV files; the time required to do this operation depends on the number of events pertaining to the selected NOI. In our simulation, since we are interested to know the connectivity of all the network nodes, we have labeled all 14 nodes as NOI.

6. Conclusion

Here we have presented *FNS*, a novel neural simulation framework based on LIFL that combines whole-brain spiking/synaptic modelling with the event-driven simulation technique, supporting neuroanatomical schemes and oriented to whole-brain realistic simulations. FNS gives the opportunity to generate models with heterogeneous regions (in the sense of both neuron parameters and local connectivity), fibre tracts (initializable on the basis of real structural data) and synaptic plasticity (STDP with different parameter sets for each node); in addition, it enables the introduction of various types of stimuli and the extraction of outputs at different network stages, depending on the kind of activity the user wants to reconstruct. With the aim of showing to the reader a simulation example, we have synthesized a subject-specific brain model sized on real structural data, and analyzed the network spontaneous activity (Sect. 5); the comparison with real MEG data shows that FNS is able to reproduce the patterns of neuromagnetic brain sources.

Dynamic models of brain activity can help us to understand the fundamental mechanisms that underpin neural processes, and relate these processes to neural data. Among the different existing approaches, SNN-based brain simulators are the only ones that can allow a structure-function mapping at the level of single neurons/synapses, offering a multi-level perspective of brain dynamics. Being based on a realistic neuron model and precise simulation technique, FNS is able to offer accurate simulations; at the same moment, the asynchronous approach and the parallel architecture make it also fast and efficient, making it possible to use it on a normal PC. This, in addition

to the fact that it is downloadable for free, make FNS a real opportunity to face large-scale brain simulations with limited budget and time. This allows to afford brain simulation in many environments, enabling us to conduct investigation in a multitude of application fields:

- development of *electrophysiological biomarkers* and improved diagnosis. Through simulations it is possible to explore unlimited structural scenarios, with the purpose of finding patterns able to distinguish healthy from non-healthy subjects, or better yet, to point out the presence of specific diseases observing at the functional level only, searching for disease-induced spatially-selective modifications, as proved in recent works (Crossley et al., 2014; Morabito et al., 2015; Capecchi et al., 2016). This could give subject-related additional information directly from real-time computer analysis of routine electrophysiological recordings, expanding the range of biomarkers available to date in scientific literature (e.g., Pineda-Pardo et al., 2014);
- test-benching for neuroprosthetic devices and neurosurgery interventions (e.g., in epilepsy). In addition, the possibility to evaluate the impact of parameter variation on network dynamics both in static and longitudinal scenarios can be exploited in drug design;
- validation of *dynamics on networks* theories and hypotheses (Schmidt et al., 2014). In particular it can be used for the investigation of brain compensation and reorganization mechanisms (Buldu et al., 2011; Abuhassan et al., 2014), evaluating longitudinal implications of structure modifications on the emerging dynamics (and viceversa), arising from the plasticity-induced network modification. The possibility to inject custom spike trains and then to mimic sensory-like processed data allow the investigation of sensorial degeneration-related consequences, e.g., if prolonged deficiencies of sensory systems can contribute to the development of some diseases, as hearing loss and Alzheimer’s disease (Hung et al., 2015);
- increase of reliability of functional and effective connectivity metrics. The model ideally gives us the opportunity to observe brain activity without spurious effects inevitably present in non-invasive electrophysiological recording techniques (e.g., *zero-lag* due to volume conduction Colclough et al., 2016). We can combine information from the model

dynamics to existent spatial filtering methods, in order to suppress spurious contributions from pre-selected non-genuine cortical sources (as the *nulling beamforming*, see Hui et al., 2010).

Future improvements of the software will regard the consideration of architecture and orientation of cortical neurons (see Mazzone et al., 2015), automatized data-driven tuning process of model parameters (see Liang and Wang, 2017), and compatibility with existent connectivity estimation tools, e.g., *Hermes* (Niso et al., 2013).

Although a simulation test has been conducted and commented, this document is not intended as user guide, but as an explanation of the mathematical operation and structure of the simulator. The reader can find the software package and technical documentation on the FNS website: www.fnsneuralsimulator.org

Acknowledgments

GS acknowledges financial support by the spanish Ministry of Economy and Competitiveness MINECO; EP acknowledges financial support by the spanish Ministry of Economy and Competitiveness MINECO [TEC2016-80063-C3-2-R]. We acknowledge Jose Ángel Pineda-Pardo for the structural data and giving us valuable comments on the manuscript.

Supplemental information

Appendix A: T_r calculation

Referring to Fig. A1, at the time the neurons inner state is altered from a second input (here excitatory, but non influential to calculation purposes), the *intermediate state* S_i is determined, and then T_r is calculated. -

In event-driven, network elements are updated only when they receive or emit a spike. Once an input spike arrives in active mode, the S_i is calculated on the basis of the time remaining to the spike generation.

Referring to the generic inner state S_i the firing equation is:

$$t_{f,i} = \frac{a}{S_i - 1} - b \tag{A1}$$

We define:

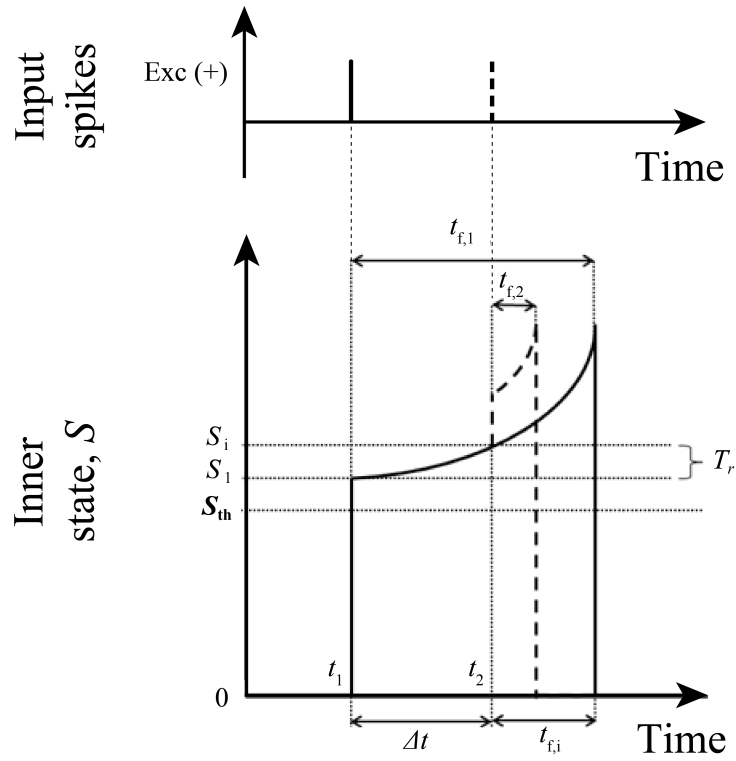


Figure A1. Representation of T_r . LIFL neuron in active mode is characterized by a spontaneous growth of S . If a pulse arrives before the actual spike generation, S is modified and the t_f will be recalculated. The recalculation considers the intermediate state S_i , i.e., the neuron state at the time the pulse arrives.

$$\Delta t = t_2 - t_1 \quad (\text{A2})$$

where t_1 and t_2 represent the arrival instants of the synaptic pulses to the considered neuron. Then:

$$t_{f,i} = t_{f,1} - \Delta t \quad (\text{A3})$$

Rearranging Eq. A1, we obtain:

$$S_i = \frac{a}{t_{f,i} + b} + 1 \quad (\text{A4})$$

Now we combine Eq. A3 with Eq. A4

$$S_i = \frac{a}{t_{f,1} - \Delta t + b} + 1 \quad (\text{A5})$$

By defining

$$T_r = S_i - S_1 \quad (\text{A6})$$

where

$$S_1 = \frac{1}{(t_{f,1} + b)} + 1 \quad (\text{A7})$$

and putting Eq. A5 in Eq. A7, we obtain:

$$T_r = \frac{a}{t_{f,1} - \Delta t + b} - \frac{a}{t_{f,1} + b} \quad (\text{A8})$$

that can be rearranged as

$$T_r = \frac{a\Delta t}{(t_{f,1} + b - \Delta t)(t_{f,1} + b)} \quad (\text{A9})$$

Note that we are interested in determining an intermediate state; this implies that we consider the second synaptic pulse only if its timing (i.e., t_2) falls before the spike occurs. This gives us:

$$\Delta t < t_{f,1} \quad (\text{A10})$$

thus we do not have restrictions from the denominator of A9.

The relation A9 can be generalized to the case as more input modify the firing time; then, we can write

$$T_r = S_{ic} - S_{ip} = \frac{a\Delta t_i}{(t_{f,ip} + b - \Delta t_i)(t_{f,ip} + b)} \quad (\text{A11})$$

with

$$\Delta t_i = t_{ic} - t_{ip} \quad (\text{A12})$$

where the subscript ip stays for *intermediate-previous* and ic for *intermediate-current*.

We can also make explicit the dependence of T_r from the previous state, by inverting $t_{f,ip}$ through Eq. A1, obtaining:

$$T_r = \frac{(S_{ip} - 1)^2 \Delta t}{a - (S_{ip} - 1) \Delta t} \quad (\text{A13})$$

Obviously, the same considerations on the arrival time of the second pulse remain valid, thus we do not have restrictions imposed by the denominator of A13.

Appendix B: LIFL Features

LIFL neuron supports natively the following neurophysiological properties: *integrator*, *spike latency*, *tonic spiking* and *class 1 excitability*. In particular, we illustrate here tonic spiking and class 1 excitability behaviors exhibited by the neuron model, obtained by the implementation of the neuron equations in MATLAB environment.

- *Tonic Spiking.* This behavior takes place when a neuron fires a continuous spike train when stimulated through a DC current input (Izhikevich, 2004). We show this property stimulating a single neuron with a constant spike train (i.e., a discretized DC current input) with amplitude A_c . The raster plot of the spiking neuron activity (i.e., the output neuron response) is reported in Fig. B1. Note that the firing frequency of the neuron is constant.
- *Class 1 Excitability.* Some cortical neurons exhibit a tonic spiking frequency that depends on the input strength, ranging from 2 Hz to 200 Hz or more. In particular, Class 1 excitability is the neuron ability to fire at low-frequency when the input is weak. This property allows neurons to encode the input strength into their firing rate (Izhikevich, 2004). In Fig. B1, we show this behavior stimulating a neuron with a ramp input with linear decay. Of course, in this case the firing frequency of the neuron is not constant.

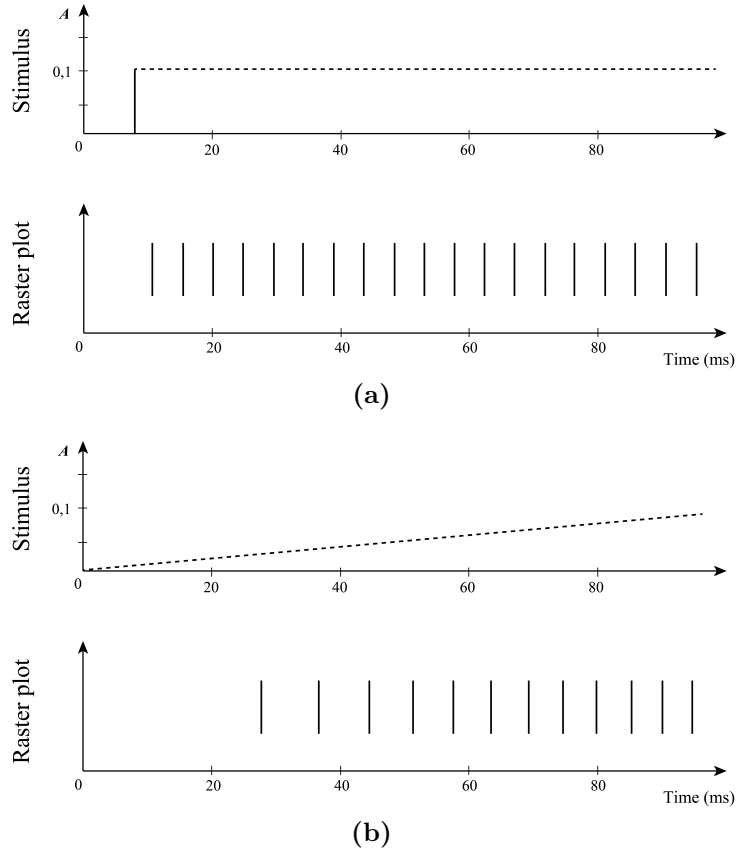


Figure B1. (a): *Tonic Spiking* behavior of LIFL neuron (basic configuration). Top: *DC* input stimulus with $A_c = 0.1$. Bottom: raster plot (firing activity) of the stimulated neuron, with respect to (simulated) biological time.

(b): *Class 1 Excitability* behavior of LIFL neuron (basic configuration). Top: *ramp* input stimulus with slope = 0.001. Bottom: raster plot (firing activity) of the stimulated neuron, with respect to (simulated) biological time.

Note that, in order to introduce the external inputs to the event-driven system, we used discrete versions of DC and ramp signals, sampled at constant intervals of $dt = 0.1$ model time

In order to further improve the realism of the LIFL neuron, some adjustments can be made at the programming level (as we do for the *refractory period*), obtaining other computational features as, for example, *tonic bursting* and *mixed mode* (Izhikevich, 2004).

Appendix C: types of distributions used in the model

In FNS Gaussian distributions are implemented both for the initialization of intra-module weights of modules (one set for excitatory and one set for inhibitory) and inter-module weights of each edge:

$$f(W) = \frac{1}{\sqrt{2\pi\sigma_W^2}} \exp\left(\frac{-(W - \mu_W)^2}{2\sigma_W^2}\right) \quad (\text{C1})$$

where μ_W is the mean, and σ_W^2 is the variance of the distribution. In the formula, W is intended to represent w (distribution of intra-module weights) or ω (distribution of intermodule weights).

In time, a gamma distribution is implemented for inter-module lengths, which reflects on a gamma distribution of delays. Such gamma distribution is characterized from parameters μ_λ (i.e., *mean parameter*) and α_λ (i.e., *shape parameter*). If we call λ the (axonal) delay, the probability density function of a gamma distribution can be written as:

$$f(\lambda) = \lambda^{\alpha_\lambda - 1} \frac{\exp(-\lambda/\mu_\lambda)}{(\mu_\lambda/\alpha_\lambda)^{\alpha_\lambda} \Gamma(\alpha_\lambda)} \quad (\text{C2})$$

Note that μ_λ can be defined as:

$$\mu_\lambda = \alpha_\lambda \theta \quad (\text{C3})$$

where θ is known as the *scale parameter*.

Note that with the parameter α_λ is possible to control the type of distribution (low α_λ values lead toward the exponential distribution; high α_λ values lead toward the dirac distribution); the more α_λ is high, the more the distribution *mode* approaches μ_λ (from the left).

Appendix D: Pseudo-code procedure

- let `spike_queue` be the list of all spikes generated by any firing neuron sorted in ascending order of spike time (the first spike in the list is the one with the least spike time);

- let `outer_burning_event`: the list of spikes to be delivered to burning neurons belonging to outer nodes. At each synchronization:
 1. each entry of this list is read and sent to the thread executing the routine for the right node;
 2. after each item in the list has been sent, the whole list is cleared.
- let `current_time` be the current simulated time;
- let `split_stop_time` be the stop time for the current BOP simulation;
- let `final_stop_time` be the simulated time at which the whole simulation must stop;
- let `run_burning_routine(s*)` be the routine which calculates all the burning events caused by the fire event hold by the spike `s*`: during this procedure, all the burning events involving burning neurons of outer nodes are stored to a special `outer_burning_event`;
- let `send_fires_for_outer_nodes()` be the routine which sends the spikes stored in `outer_burning_event` to burning neurons in outer nodes;
- let `update_incoming_spikes_queue()` be the routine which updates the `spike_queue` with the spikes coming from outer nodes and targeting burning neurons of the present node before beginning the next BOP simulation.

```

while true:
while current_time < split_stop_time:
s* = spike_queue.pop()
run_burning_routine(s*)
if current_time >= split_stop_time: (1)
if split_stop_time >= final_stop_time: (2)
return
send_fires_for_outer_nodes()
wait_until(current_time < split_stop_time) (3)
update_spikes_queue()

```

- (1) end of the BOP: send the fires to the outer nodes
- (2) end of the last BOP: end of the node simulation

(3) stops the thread until `split_stop_time` is updated
with the next BOP stop time

7. Bibliography

References

- Abbott, L. F., Nelson, S. B., 2000. Synaptic plasticity: taming the beast. *Nature Neuroscience* 3, 1178–1183.
- Abuhassan, K., Coyle, D., Maguire, L., 2014. Compensating for thalamo-cortical synaptic loss in Alzheimer’s disease. *Frontiers in computational neuroscience* 8 (65).
URL <https://doi.org/10.3389/fncom.2014.00065>
- Acciarito, S., Cardarilli, G., Cristini, A., Di Nunzio, L., Fazzolari, R., Khanal, G., Re, M., Susi, G., 2017. Hardware design of LIF with latency neuron model with memristive STDP synapses. *Integration, the VLSI Journal* 59, 81–89.
- Barardi, A., Sancristbal, B., Garcia-Ojalvo, J., 2014. Phase-coherence transitions and communication in the gamma range between delay-coupled neuronal populations. *PLOS Computational Biology* 10 (7), e22561.
URL <https://doi.org/10.1371/journal.pcbi.1003723>
- Bassett, D., Bullmore, E., Verchinski, B. A., Mattay, V. S., Weinberger, D. R., Meyer-Lindenberg, A., 2008. Hierarchical organization of human cortical networks in health and schizophrenia. *J Neurosci* 28 (37), 9239–9248.
- Bi, G., Poo, M., 1998. Synaptic modifications in cultured hippocampal neurons: dependence on spike timing, synaptic strength, and postsynaptic cell type. *The Journal of Neuroscience* 18 (24), 10464–10472.
- Bohland, J., Wu, C., Barbas, H., Bokil, H., Bota, M., Breiter, H., Cline, H., Doyle, J., Freed, P., Greenspan, R., Haber, S., Hawrylycz, M., Herrera, D., Hilgetag, C., Huang, Z., Jones, A., Jones, E., Karten, H., Kleinfeld, D., Ktter, R., Lester, H., Lin, J., Mensh, B., Mikula, S., Panksepp, J., Price, J., Safdieh, J., Saper, C., Schiff, N., Schmahmann, J., Stillman, B.,

- Svoboda, K., Swanson, L., Toga, A., Van Essen, D., Watson, J., Mitra, P., 2009. A proposal for a coordinated effort for the determination of brainwide neuroanatomical connectivity in model organisms at a mesoscopic scale. *PLOS Computational Biology* 5 (3), 1–9.
URL <https://doi.org/10.1371/journal.pcbi.1000334>
- Branzoli, F., Ercan, E., Valabregue, R., Wood, E., Buijs, M., Webb, A., Ronen, I., 2016. Differentiating between axonal damage and demyelination in healthy aging by combining diffusion-tensor imaging and diffusion-weighted spectroscopy in the human corpus callosum at 7T. *Neurobiology of Aging* 47, 210–217.
- Brette, R., 2006. Exact simulation of integrate-and-fire models with synaptic conductances. *Neural Computation* 18 (8), 2004–2027.
- Brette, R., 2007. Exact simulation of integrate-and-fire models with exponential currents. *Neural Computation* 19 (10), 2604–2609.
- Brette, R., Goodman, D., 2016. Brian Documentation. Release 1.4.3.
URL <http://www.briansimulator.org>
- Brette, R., Rudolph, M., Carnevale, T., Hines, H., Beeman, D., Bower, J. M., Diesmann, M., Morrison, A., Goodman, P. H., Jr Harris, F. C., Zirpe, M., Natschläger, T., Pecevski, D., Ermentrout, B., Djurfeldt, M., Lansner, A., Rochel, O., Vieville, T., Muller, E., Davison, A. P., El Boustani, S., Destexhe, A., 2007. Simulation of networks of spiking neurons: A review of tools and strategies. *Journal of Computational Neuroscience* 23 (3), 349–398.
- Brookes, M., Hale, J., Zumer, J., Stevenson, C., Francis, S., Barnes, G., Owen, J., Morris, P., Nagarajan, S., 2011. Measuring functional connectivity using MEG: Methodology and comparison with fcMRI. *Neuroimage* 56 (3), 1082–1104.
URL <https://doi.org/10.1016/j.neuroimage.2011.02.054>
- Brookes, M., Woolrich, M., Barnes, G., 2012. Measuring functional connectivity in MEG: a multivariate approach insensitive to linear source leakage. *Neuroimage* 2, 910–920.
URL <https://doi.org/10.1016/j.neuroimage.2012.03.048>

- Buldu, J. M., Bajo, R., Maestú, F., Castellanos, N., Leyva, I., Gil, P., Sendia-Nadal, I., Almendral, J. A., Nevado, A., del Pozo, F., Boccaletti, S., 2011. Reorganization of functional networks in mild cognitive impairment. *PLOS ONE* 6 (5), 1–8.
URL <https://doi.org/10.1371/journal.pone.0019584>
- Buzsaki, G., Anastassiou, C., Koch, C., 2012. The origin of extracellular fields and currents - EEG, ECoG, LFP and spikes. *Nat Rev Neurosci* 13, 407–420.
- Cabral, J., Hugues, E., Sporns, O., Deco, G., 2011. Role of local network oscillations in resting-state functional connectivity. *Neuroimage* 57, 130–139.
URL <https://doi.org/10.1016/j.neuroimage.2011.04.010>
- Cabral, J., Luckhoo, H., Woolrich, M., Joensson, M., Mohseni, H., Baker, A., Kringelbach, M., Deco, G., 2014. Exploring mechanisms of spontaneous functional connectivity in MEG: How delayed network interactions lead to structured amplitude envelopes of band-pass filtered oscillations. *Neuroimage* 90, 423–435.
URL <https://doi.org/10.1016/j.neuroimage.2013.11.047>
- Capecci, E., Doborjeh, Z., Mammone, N., Foresta, F., Morabito, F., Kasabov, N., 2016. Longitudinal study of Alzheimer’s disease degeneration through EEG data analysis with a NeuCube spiking neural network model. In: 2016 International Joint Conference on Neural Networks (IJCNN). IEEE, pp. 1360–1366.
- Caporale, N., Dan, Y., 2008. Spike timing-dependent plasticity: a Hebbian learning rule. *Annu Rev Neurosci*. 31, 25–46.
- Cardarilli, G. C., Cristini, A., Di Nunzio, L., Re, M., Salerno, M., Susi, G., 2013. Spiking neural networks based on LIF with latency: Simulation and synchronization effects. In: 2013 Asilomar Conference on Signals, Systems and Computers. IEEE, Pacific Grove, CA, USA, pp. 1838–1842.
- Colclough, G., Woolrich, M., Tewarie, P., Brookes, M., Quinn, A., Smith, S., 2016. How reliable are MEG resting-state connectivity metrics? *Neuroimage* 138, 284–293.
URL <https://doi.org/10.1016/j.neuroimage.2016.05.070>

- Coombes, S., 2006. Neural fields. *Scholarpedia* 1 (6), 1373.
- Cormen, T., Leiserson, C., Rivest, R., Stein, C., 2001. *Introduction to algorithms*, 2nd ed. The MIT Press.
- Cristini, A., Salerno, M., Susi, G., 2015. A continuous-time spiking neural network paradigm. In: Bassis, S., Esposito, A., Morabito, F. C. (Eds.), *Advances in Neural Networks: Computational and Theoretical Issues*. Springer International Publishing, pp. 49–60.
- Crossley, N. A., Mechelli, A., Scott, J., Carletti, F., Fox, P. T., McGuire, P., Bullmore, E. T., 2014. The hubs of the human connectome are generally implicated in the anatomy of brain disorders. *Brain* 137 (8), 2382–2395.
URL <http://dx.doi.org/10.1093/brain/awu132>
- David, O., Friston, J., 2003. A neural mass model for MEG/EEG: coupling and neuronal dynamics. *Neuroimage* 20, 1743–1755.
URL <https://doi.org/10.1016/j.neuroimage.2003.07.015>
- de Pasquale, F., Della Penna, S., Snyder, A. Z., Lewis, C., Mantini, D., Marzetti, L., Belardelli, P., Ciancetta, L., Pizzella, V., Romani, G. L., Corbetta, M., 2010. Temporal dynamics of spontaneous MEG activity in brain networks. *Proceedings of the National Academy of Sciences USA* 107 (13), 6040–6045.
- Deco, G., Jirsa, V., 2012. Ongoing cortical activity at rest: Criticality, multistability, and ghost attractors. *The Journal of Neuroscience* 32 (10), 3366–3375.
- Deco, G., Jirsa, V., Robinson, P. A., Breakspear, M., Friston, K., 2008. The dynamic brain: From spiking neurons to neural masses and cortical fields. *PLOS Comput Biol* 4, 1–35.
URL <https://doi.org/10.1371/journal.pcbi.1000092>
- Delorme, A., Thorpe, S., 2003. SpikeNET: an event-driven simulation package for modelling large networks of spiking neurons. *Network Computation in Neural Systems* 14 (4), 613–627.
- Desikan, R., Segonne, F., Fischl, B., Quinn, B., Dickerson, B., Blacker, D., Buckner, R., Dale, A., Maguire, R., Hyman, B., Albert, M., Killiany, R., 2006. An automated labeling system for subdividing the human cerebral

- cortex on MRI scans into gyral based region of interests. *Neuroimage* 31, 968–980.
URL <https://doi.org/10.1016/j.neuroimage.2006.01.021>
- D’Haene, M., 2006. A framework for parallel event driven simulation of large spiking neural networks. In: 7e FirW Doctoraatssymposium.
- D’Haene, M., Hermans, M., Schrauwen, B., 2014. Toward unified hybrid simulation techniques for spiking neural networks. *Neural Comput.* 26 (6), 1055–79.
- Djurfeldt, M., Johansson, C., Ekeberg, O., Rehn, M., Lundqvist, M., Lansner, A., 2005. Massively parallel simulation of brain-scale neural network models. Tech. rep., “KTH” School of Computer Science and Communication, Stockholm, Sweden.
- Finger, H., Bnstrup, M., Cheng, B., Mess, A., Hilgetag, C., Thomalla, G., Gerloff, C., Knig, P., 08 2016. Modeling of large-scale functional brain networks based on structural connectivity from DTI: Comparison with EEG derived phase coupling networks and evaluation of alternative methods along the modeling path. *PLOS Computational Biology* 12 (8), 1–28.
URL <https://doi.org/10.1371/journal.pcbi.1005025>
- Fischl, B., 2012. Freesurfer. *Neuroimage* 62 (2), 774–781.
URL <https://doi.org/10.1016/j.neuroimage.2012.01.021>
- FitzHugh, R., 1955. Mathematical models of threshold phenomena in the nerve membrane. *Bulletin of Mathematical Biology* 17 (4), 257–278.
- Fontaine, B., Peremans, H., 2009. Bat echolocation processing using first-spike latency coding. *Neural Networks* 22 (10), 1372 – 1382.
- Fourcaud-Trocme, N., Hansel, D., van Vreeswijk, C., Brunel, N., 2003. How spike generation mechanisms determine the neuronal response to fluctuating inputs. *The Journal of Neuroscience* 23 (5), 11628–11640.
- Frohlich, F., Bazhenov, M., Sejnowski, T. J., 2008. Pathological effect of homeostatic synaptic scaling on network dynamics in diseases of the cortex. *The Journal of Neuroscience: The Official Journal of the Society for Neuroscience* 28 (7), 1709–1720.

- Garces, P., Pineda, J.-A., Canuet, L., Aurtenetxe, S., Lopez, M. E., Marcos, A., Yus, M., Llanero-Luque, M., del Pozo, F., Sancho, M., Maestú, F., 2014. The Default Mode Network is functionally and structurally disrupted in amnesic mild cognitive impairment - a bimodal MEG DTI study. *Neuroimage Clin.* 6, 214–221.
URL <https://doi.org/10.1016/j.nicl.2014.09.004>
- Gerstner, W., Kistler, W., Naud, R., Paninski, L., 2014. *Neuronal Dynamics. From single neurons to networks and models of cognition.* Cambridge University Press.
- Gewaltig, M., Diesmann, M., 2007. NEST (NEural Simulation Tool). *Scholarpedia* 2 (4), 1430.
- Gollisch, T., Meister, M., 2008. Rapid neural coding in the retina with relative spike latencies. *Science* 319 (5866), 1108–1111.
URL <http://science.sciencemag.org/content/319/5866/1108>
- Gollo, L., Copelli, M., Roberts, J. A., 2016. Diversity improves performances in excitable networks. *PeerJ* 4, e1912.
URL <https://doi.org/10.7717/peerj.1912>
- Gollo, L., Mirasso, C., Sporns, O., Breakspear, M., 2014. Mechanisms of zero-lag synchronization in cortical motifs. *PLOS computational biology* 10 (4), 1–17.
URL <https://doi.org/10.1371/journal.pcbi.1003548>
- Gollo, L., Mirasso, C., Villa, A., 2010. Dynamic control for synchronization of separated cortical areas through thalamic relay. *NeuroImage* 52 (3), 947–955.
URL <https://doi.org/10.1016/j.neuroimage.2009.11.058>
- Grassmann, C., Anlauf, J., 1998. Distributed, event driven simulation of spiking neural networks. In: *Proceedings of the International ICSC - IFAC Symposium on Neural Computation.* pp. 100–105.
- Hagmann, P., 2005. *From diffusion MRI to brain connectomics.* Dissertation, Lausanne: EPFL.
URL <https://infoscience.epfl.ch/record/33696>

- Hagmann, P., Cammoun, L., Gigandet, X., Meuli, R., Honey, C., Wedeen, V., Sporns, O., 2008. Mapping the structural core of human cerebral cortex. *Plos Biology* 6 (7), 1–15.
URL <https://doi.org/10.1371/journal.pbio.0060159>
- Hanuschkin, A., Kunkel, S., Helias, M., Morrison, A., Diesmann, M., 2010. A general and efficient method for incorporating precise spike times in globally time-driven simulations. *Frontiers in Neuroinformatics* 4 (113).
URL <https://doi.org/10.3389/fninf.2010.00113>
- Heeger, D., Heeger, P. D., 2000. Poisson model of spike generation.
URL <http://citeseerx.ist.psu.edu/viewdoc/summary?doi=10.1.1.37.6580>
- Hines, M. L., Carnevale, N. T., 1997. The NEURON simulation environment. *Neural Computation* 9 (6), 1179–1209.
- Hipp, J., Hawellek, D., Corbetta, M., Siegel, M., Engel, A., 2012. Large-scale cortical correlation structure of spontaneous oscillatory activity. *Nature Neuroscience* 15, 884–890.
- Hodgkin, A. L., Huxley, A. F., 1952. A quantitative description of membrane current and application to conduction and excitation in nerve. *The Journal of Physiology* 117 (4), 500–544.
- Hui, H., Pantazis, D., Bressler, S., Leahy, R., 2010. Identifying true cortical interactions in MEG using the nulling beamformer. *Neuroimage* 49 (4), 3161–3174.
URL <https://doi.org/10.1016/j.neuroimage.2009.10.078>
- Hung, S., Liao, K., Muo, C., Lai, S., Chang, C., Hung, H., 2015. Hearing loss is associated with risk of Alzheimers disease: A case-control study in older people. *Journal of Epidemiology* 25 (8), 517–521.
- Izhikevich, E., Gally, J., Edelman, G., 2004. Spike-timing dynamics of neuronal groups. *Cereb Cortex*. 14 (8), 933–944.
- Izhikevich, E. M., 2003. Simple model of spiking neurons. *IEEE Transaction on Neural Networks* 14 (6), 1569–1572.

- Izhikevich, E. M., 2004. Which model to use for cortical spiking neurons? *IEEE Transaction on Neural Networks* 15 (5), 1063–1070.
- Izhikevich, E. M., 2007. *Dynamical systems in neuroscience: the geometry of excitability and bursting*. Computational neuroscience. MIT Press, Cambridge, Mass., London.
- Kempler, R., Gerstner, W., van Hemmen, J. L., 1999. Hebbian learning and spiking neurons. *Physical Review E* 59 (4), 4498–4514.
- Liang, H., Wang, H., 01 2017. Structure-function network mapping and its assessment via persistent homology. *PLOS Computational Biology* 13 (1), 1–19.
URL <https://doi.org/10.1371/journal.pcbi.1005325>
- Lobb, C., Chao, Z., Fujimoto, RM, Potter, S., 2005. Parallel event-driven neural network simulations using the hodgkin-huxley neuron model. In: *Principles of Advanced and Distributed Simulation (PADS)*. pp. 16–25.
- Lubachevsky, B., 1989. Efficient distributed event-driven simulations of multiple-loop networks. *Communications of the ACM* 32 (1), 111–123.
- Maslennikov, O. V., Nekorkin, V. I., Jul 2014. Modular networks with delayed coupling: Synchronization and frequency control. *Phys. Rev. E* 90, 012901.
- Mattia, M., Del Giudice, P., 2000. Efficient event-driven simulation of large networks of spiking neurons and dynamical synapses. *Neural Computation* 12 (10), 2305–2329.
- Mazzoni, A., Lindn, H., Cuntz, H., Lansner, A., Panzeri, S., Einevoll, G. T., 12 2015. Computing the local field potential (LFP) from integrate-and-fire network models. *PLOS Computational Biology* 11 (12), 1–38.
URL <https://doi.org/10.1371/journal.pcbi.1004584>
- Mazzoni, A., Panzeri, S., Logothetis, N., Brunel, N., 12 2008. Encoding of naturalistic stimuli by local field potential spectra in networks of excitatory and inhibitory neurons. *PLOS Computational Biology* 4 (12), 1–20.
URL <https://doi.org/10.1371/journal.pcbi.1000239>
- Morabito, F. C., Campolo, M., Labate, D., Morabito, G., Bonanno, L., Bramanti, A., de Salvo, S., Marra, A., Bramanti, P., 2015. A longitudinal

- EEG study of Alzheimer's disease progression based on a complex network approach. *International Journal of Neural Systems* 25 (02), 1550005.
URL <http://www.worldscientific.com/doi/abs/10.1142/S0129065715500057>
- Morrison, A., Straube, S., Plesser, H., Diesmann, M., 2006. Exact subthreshold integration with continuous spike times in discrete time neural network simulations. *Neural Computation* 19, 47–79.
- Mouraud, A., Puzenat, D., 2009. Simulation of large spiking neural networks on distributed architectures. the DAMNED simulator. In: Palmer-Brown, D., Draganova, C., Pimenidis, E., Mouratidis, H. (Eds.), *Engineering Applications of Neural Networks*. Springer International Publishing, pp. 359–370.
- Nakagawa, T., Woolrich, M., Luckhoo, H., Joensson, M., Mohseni, H., Kringelbach, M., Jirsa, V., Deco, G., 2014. How delays matter in an oscillatory whole-brain spiking-neuron network model for MEG alpha-rhythms at rest. *Neuroimage* 87, 383–394.
URL <https://doi.org/10.1016/j.neuroimage.2013.11.009>
- Niso, G., Bruña, R., Pereda, E., Gutiérrez, R., Bajo, R., Maestú, F., del Pozo, F., 2013. HERMES: Towards an integrated toolbox to characterize functional and effective brain connectivity. *Neuroinformatics* 11 (4), 405–434.
- Pecevski, D., Kappel, D., Jonke, Z., 2014. NEVESIM: event-driven neural simulation framework with a python interface. *Frontiers in Neuroinformatics* 8 (70).
URL <http://journal.frontiersin.org/article/10.3389/fninf.2014.00070>
- Pineda-Pardo, J., Bruña, R., Woolrich, R., Marcos, A., Nobre, A., Maestú, F., Vidaurre, D., 2014. Guiding functional connectivity estimation by structural connectivity in MEG: an application to discrimination of conditions of mild cognitive impairment. *Neuroimage* 101, 765–77.
URL <https://doi.org/10.1016/j.neuroimage.2014.08.002>
- Pinotsis, D., Robinson, P., beim Graben, P., Friston, K., 2014. Neural masses and fields: modeling the dynamics of brain activity. *Frontiers in*

- Computational Neuroscience 8 (149).
URL <http://journal.frontiersin.org/article/10.3389/fncom.2014.00149>
- Ponge, J., 2011. Fork and join: Java can excel at painless parallel programming too! Oracle technology network.
URL <http://www.oracle.com/technetwork/articles/java/fork-join-422606.html>
- Raichle, M., MacLeod, A. M., Snyder, A. Z., Powers, W. J., Gusnard, D. A., Shulman, G. L., 2001. A default mode of brain function. *Proceedings of the National Academy of Sciences USA* 98 (2), 676–682.
- Riecke, H., Roxin, A., Madruga, S., Solla, S., 2007. Multiple attractors, long chaotic transients, and failure in small-world networks of excitable neurons. *Chaos* 17 (2).
URL <https://doi.org/10.1063/1.2743611>
- Ros, E., Carrillo, R., Ortigosa, E., Barbour, B., Agís, R., 2006. Event-driven simulation scheme for spiking neural networks using lookup tables to characterize neuronal dynamics. *Neural Computation*.
- Rudolph-Lilith, M., Dubois, M., Destexhe, A., 2012. Analytical integrate-and-fire neuron models with conductance-based dynamics and realistic postsynaptic potential time course for event-driven simulation strategies. *Neural Comput.* 24 (6), 1426–1461.
- Salerno, M., Susi, G., Cristini, A., 2011. Accurate latency characterization for very large asynchronous spiking neural networks. In: Pellegrini, M., Fred, A. L. N., Filipe, J., Gamboa, H. (Eds.), *BIOINFORMATICS 2011 - Proceedings of the International Conference on Bioinformatics Models, Methods and Algorithms*. SciTePress, pp. 116–124.
- Sanz Leon, P., Knock, S., Marmaduke Woodman, M., Domide, L., Mersmann, J., McIntosh, A., Jirsa, V., 2013. The virtual brain: a simulator of primate brain network dynamics. *Frontiers in Neuroinformatics*. 7, 10.
URL <https://www.frontiersin.org/article/10.3389/fninf.2013.00010>

- Scheffler, L., 2015. NeuroOS and NeuroBlocks a neural/cognitive operating system and building blocks. *Biologically Inspired Cognitive Architectures* 4, 75–105.
- Schmidt, H., Petkov, G., Richardson, M. P., Terry, J. R., 2014. Dynamics on networks: The role of local dynamics and global networks on the emergence of hypersynchronous neural activity. *PLOS Computational Biology* 10 (11), 1–16.
URL <https://doi.org/10.1371/journal.pcbi.1003947>
- Sjöström, J., Gerstner, W., 2010. Spike-timing dependent plasticity. http://www.scholarpedia.org/article/Spike-timing_dependent_plasticity.
- Smith, K., 1994. Conduction properties of central demyelinated and remyelinated axons, and their relation to symptom production in demyelinating disorders. *Nature (eye)* 8 (2), 224–237.
- Sporns, C., Tononi, G., Kötter, R., 09 2005. The human connectome: A structural description of the human brain. *PLOS Computational Biology* 1 (4).
URL <https://doi.org/10.1371/journal.pcbi.0010042>
- Susi, G., 2015. Bio-inspired temporal-decoding network topologies for the accurate recognition of spike patterns. *Transactions on Machine Learning and Artificial Intelligence* 3 (4), 27–41.
- Susi, G., Cristini, A., Salerno, M., 2016. Path multimodality in Feedforward SNN module, using LIF with latency model. *Neural Network World* 26 (4), 363–376.
- Susi, G., Ye-Chen, S., de Frutos Lucas, J., Niso, G., Maestú, F., 2018. Neurocognitive aging and functional connectivity using magnetoencephalography. In: *Oxford research encyclopedia of psychology and aging*. Oxford University press, Oxford.
- Thivierge, J., 2008. Neural diversity creates a rich repertoire of brain activity. *Communicative & Integrative Biology* 1, 188–189.

- Ton, R., Deco, G., Daffertshofer, A., 2014. Structure-function discrepancy: Inhomogeneity and delays in synchronized neural networks. *PLOS Computational Biology* 10 (7), 1–15.
- Tonnelier, A., Belmabrouk, H., Martinez, D., 2007. Event-driven simulations of nonlinear integrate-and-fire neurons. *Neural Comput.* 19 (12), 1426–1461.
- Trotta, L., Franci, A., Sepulchre, R., 2013. First spike latency sensitivity of spiking neuron models. *BMC Neuroscience* 14 (1), 354.
- van Rossum, M. C., Shippi, M., Barrett, A. B., 2012. Soft-bound synaptic plasticity increases storage capacity. *PLOS Computational Biology* 8 (12), 1–11.
URL <https://doi.org/10.1371/journal.pcbi.1002836>
- Van Veen, B., van Drongelen, W., Yuchtman, M., Suzuki, A., 1997. Localization of brain electrical activity via linearly constrained minimum variance spatial filtering. *IEEE Transactions on Biomedical Engineering* 44, 867–880.
- Vicente, R., Gollo, L. L., Mirasso, C. R., Fischer, I., Pipa, G., 2008. Dynamical relaying can yield zero time lag neuronal synchrony despite long conduction delays. *Proceedings of the National Academy of Sciences USA* 105 (44), 17157–17162.
- Vilela, R. D., Lindner, B., Sep 2009. Comparative study of different integrate-and-fire neurons: Spontaneous activity, dynamical response, and stimulus-induced correlation. *Phys. Rev. E* 80, 031909.
URL <http://link.aps.org/doi/10.1103/PhysRevE.80.031909>
- Viriyopase, A., Bojak, I., Zeitler, M., Gielen, S., 2012. When long-range zero-lag synchronization is feasible in cortical networks. *Frontiers in computational neuroscience* 6, 49.
URL <https://www.frontiersin.org/article/10.3389/fncom.2012.00049>
- Wang, H., Chen, Y., Chen, Y., 2013. First-spike latency in hodgkin’s three classes of neurons. *Journal of Theoretical Biology* 328, 19–25.

- Watts, J. D., Strogatz, S. H., 1998. Collective dynamics of 'small-world' networks. *Nature* 393 (1), 440–442.
- Zhu, Z., Zumer, J. M., Lowenthal, M. E., Padberg, J., Recanzone, G. H., Krubitzer, L. A., Nagarajan, S. S., Disbrow, E. A., 2009. The relationship between magnetic and electrophysiological responses to complex tactile stimuli. *BMC Neuroscience* 10 (1), 4.
URL <https://doi.org/10.1186/1471-2202-10-4>
- Zimmerman, D., Zumbo, B., Williams, R., 2003. Bias in estimation and hypothesis testing of correlation. *Psicologica* 24, 133–158.

References